Research Article

Khaled Lotfy*, Ibrahim S. Elshazly, Borhen Halouani*, Saurav Sharma, Ramdan S. Tantawi, and Eslam S. Elidy

Influence of a magnetic field on double-porosity photo-thermoelastic materials under Lord–Shulman theory

https://doi.org/10.1515/phys-2025-0154
received January 08, 2025; accepted April 03, 2025

Abstract: This study explores the influence of a magnetic field on a two-dimensional photo-thermoelastic material with a dual porous structure, based on the Lord–Shulman theory of thermoelasticity. The model presents a novel approach to understanding magneto-thermoelastic interactions in such elastic semiconductor materials. The model incorporates the Lorentz force to account for magnetoelastic interactions and considers a uniform double-porosity thermoelastic half-space. Analytical expressions for key physical quantities are derived using the normal mode analysis technique, assuming exponential representations for the variables. The governing equations for the generalized double-porosity structure of photo-thermoelastic materials, incorporating a single relaxation time, are formulated and solved under specific boundary conditions. The results provide insights into the coupled behavior of thermal, elastic, and electromagnetic fields in dual-porosity materials and highlight the significant role of magnetic fields in influencing wave propagation and stress distribution. The work underscores the critical role of magnetic fields in altering wave propagation and stress behavior, offering potential advancements in materials science and engineering applications.

Keywords: photo-thermoelasticity, L-S theory, double porosity, magnetic field, dual porous structure, wave propagation

Nomenclature

$\lambda,\ \mu$	Lame' parameters (Pa (N/m^2)
u_i	displacement vector (m)
δ_{ij}	Kronecker delta
ρ	mass density (kg/m^3)
τ_0	relaxation time (s)
τ	photogenerated carrier lifetime (s)
E_g	the energy gap of the semiconductor (eV)
C_e	specific heat at constant strain (J/(kg K))
D_E	carrier diffusion coefficient (m^2/s)
$\kappa = \frac{\partial N_0}{\partial T}\frac{1}{\tau},\ \ N_0$	carrier concentration at temperature T_0 (m^{-3})
τ_{ij}	stress tensor (Pa (N/m^2))
υ_1	volume fraction field corresponding to pores
υ_2	volume fraction field corresponding to fissures
Φ, Ψ	volume fraction fields corresponding to υ_1 and υ_2, respectively
K^*	volume coefficient of thermal expansion (W/(m K))
K	thermal conductivity (K^{-1})
k_1, k_2	acoefficients of equilibrated inertia (kg/m^3)
T_0	reference temperature (K)
$b, d, b_1, \gamma, \gamma_1\gamma_2$	constitutive coefficients (Pa (N/m^2))
σ_i	equilibrated stress corresponding to υ_1 (Pa (N/m^2))
τ_i	equilibrated stress corresponding to υ_2 (Pa (N/m^2))
T	temperature change measured at T_0 (K)

*** Corresponding author: Khaled Lotfy,** Department of Mathematics, Faculty of Science, Zagazig University, P.O. Box 44519, Zagazig, Egypt, e-mail: khlotfy_1@yahoo.com; khlotfy@zu.edu.eg
*** Corresponding author: Borhen Halouani,** Department of Mathematics, College of Science, King Saud University, P.O. Box 2455, Riyadh, 11451, Saudi Arabia, e-mail: halouani@ksu.edu.sa
Ibrahim S. Elshazly: Department of Basic Sciences, Common First Year, King Saud University, Riyadh, 11451, Saudi Arabia, e-mail: iali2.c@ksu.edu.sa
Saurav Sharma: University of Houston Cullen College of Engineering, 7900 Cambridge Street, #7-2G, Houston, Texas, 77054, United States of America, e-mail: sauravkuk@gmail.com
Ramdan S. Tantawi: Department of Mathematics, Faculty of Science, Zagazig University, P.O. Box 44519, Zagazig, Egypt, e-mail: ramadan_tantawi1@yahoo.com
Eslam S. Elidy: Department of Mathematics, Faculty of Science, Zagazig University, P.O. Box 44519, Zagazig, Egypt, e-mail: eslamelidy@yahoo.com
ORCID: Khaled Lotfy 0000-0001-9383-1361

ε_1	thermoelastic coupling parameter
ε_2	thermoenergy coupling parameter
ε_3	thermoelectric coupling parameter

1 Introduction

The study of the influence of magnetic fields on two-dimensional photo-thermoelastic materials with a dual porous structure has significant implications for real-world applications. Such materials are integral in advanced engineering and technology fields, including aerospace, biomedical devices, and geophysical exploration. Understanding their behavior under magnetic and thermal effects enables the development of sensors and actuators that operate reliably in harsh environments. For example, these materials can be used in magnetic field sensors for medical imaging or as components in devices requiring precise thermal and mechanical stability, such as energy storage systems and structural health monitoring. Moreover, the incorporation of dual porosity in the analysis allows for better modeling of materials like rocks or porous composites, which are crucial in oil extraction, carbon sequestration, and earthquake prediction. By combining theoretical advancements like the Lord–Shulman (L-S) theory and practical considerations, this study paves the way for innovations in material design and multifunctional device applications.

Photo-thermoelasticity is the study of the coupled behavior of thermal, elastic, and optical properties in materials under stress [1]. This field is particularly relevant in the analysis of complex materials, such as porous media, which exhibit intricate behaviors due to their internal structure. Double porosity [2–4] describes a material possessing two distinct pore systems, leading to complex mechanical and thermal responses. The study focuses on the interaction between light and materials subjected to thermal stress, which allows for the measurement of stress and strain using optical techniques, specifically photoelasticity. The governing equations of photo-thermoelasticity incorporate the principles of thermodynamics, elasticity, and optics. Double-porosity models are employed to characterize materials with two separate pore networks, a concept that is particularly important for materials such as rocks, soils, and certain biological tissues [5]. The two-pore systems can interact, influencing the material's overall mechanical and thermal properties. The thermal behavior in double-porosity media is complex, as the heat transport mechanisms in each pore network differ. Consequently, thermal expansion and conduction may vary significantly between the two systems, leading to heterogeneous stress distributions. The L-S theory of thermoelasticity, introduced in 1967, incorporates a single relaxation time for the thermoelastic process, accounting for the time-dependent response of the material [6].

Double porosity refers to a material with two distinct pore systems: macropores and larger pores that dominate the bulk material, and microfissures indicate smaller cracks or fissures within the material. The interaction between these two pore systems influences the material's thermal and mechanical properties, making it suitable for applications such as oil and gas extraction and geothermal energy systems. The linear theory of elastic materials with double porosity was first introduced in the publications by Barenblatt *et al.* [7,8]. Khalili and Valliappan [9] utilized the idea of flow and deformation in double-porous media. Masters *et al.* conducted a study on the correlation between temperature and a twofold porosity model of deformable porous media [10]. Khalili and Selvadurai [11] examined the comprehensive coupled constitutive model for thermo-hydro-mechanical analysis in elastic media with dual porosity. Zhao and Chen [12] presented a comprehensive dual-porosity model that is fully coupled and applicable to anisotropic formations. Svanadze [13] investigated the dynamic issues related to the theory of elasticity in solids with dual porosity. Ainouz researched the homogenized double-porosity models for poro-elastic media featuring an interfacial flow barrier [14]. Svanadze [15] conducted research on the theory of elasticity for solids with double porosity, specifically focusing on plane waves and boundary value problems. In their study, Straughan [16] examined the stability and uniqueness of elasticity in a double-porosity system.

Previously, academics have explored many issues related to magnetic fields. Mahato and Biswas [17] specifically examined the state space method, three-phase-lag model, Rayleigh waves, Eringen's nonlocal thermoelasticity, and double porosity. Berryman and Wang [18] have devised analytical and numerical techniques to solve the intricate equations that govern thermoelasticity in materials with dual porosity. Finite element analysis and boundary element techniques are frequently employed to model the response of these materials under different thermal and mechanical loads [3]. Experimental studies are essential for verifying theoretical models of thermoelasticity in double-porosity materials. Thermal loading experiments, acoustic emission monitoring, and digital image correlation techniques are used to quantify the stress and strain responses of materials having double porosity under controlled settings. The investigation of thermoelasticity in double-porosity materials holds great importance in various domains like geothermal energy extraction, petroleum engineering, and materials science. Gaining insight into the thermal and mechanical characteristics of rocks with dual porosity is crucial for maximizing the efficiency of resource extraction from underground formations. Furthermore, researchers [19]

are currently investigating synthetic materials that include customized double-porosity architectures for applications in enhanced insulation, filtration, and medicinal implants.

An essential obstacle in this domain is the intricacy of the models needed to precisely depict the behavior of double-porosity materials when subjected to thermoelastic loading. These models typically necessitate advanced numerical techniques for their resolution, which can be computationally demanding. Another difficulty lies in the integration of multiple physical processes, such as heat transport, fluid flow, and mechanical deformation, into a cohesive model. Subsequent studies could prioritize the development of more streamlined algorithms and computational strategies to manage these interconnected activities. Precisely determining the material parameters of double-porosity systems, including permeability, thermal conductivity, and elastic moduli, is crucial for enhancing the accuracy of predictive models. Progress in imaging techniques and material testing will be pivotal in this field. Double porosity models are employed to characterize materials that possess two distinct pore networks. This concept is especially significant in the examination of materials such as rocks, dirt, and certain biological tissues. Interactions between the two pore systems can have an impact on the material's overall mechanical and thermal properties. The thermal effects in porous media with double porosity are intricate because of the distinct heat transport mechanisms in the two-pore networks. The thermal expansion and conduction in the two systems might vary greatly, resulting in distinct stress distributions.

Marin and Marinescu [20] further examine dipolar thermoelastic materials, a particular case of multipolar continuum mechanics. This hypothesis posits the existence of two porosity types: macroporosity, denoting the presence of pores inside the material, and microporosity, indicating the presence of minute fissures within the porous structure. The theory of thermoelastic dynamics is analyzed for materials with a dual-porosity structure and microtemperature. This study is distinctive as it addresses an issue of double-porous thermoelastic materials with microtemperature, previously examined by Florea [21]. The originality resides in the exploration of a temporal regression problem. The research examines Rayleigh-type waves in a layered model comprising a thermoelastic material with a dual porosity structure. The dispersion relation is obtained by implementing appropriate boundary conditions, demonstrating the existence of multiple modes and the dispersive and attenuative properties of Rayleigh-type waves. The dispersion relation reduces to the dispersion equation for Stoneley-type waves when Kumar *et al.* [22] posit that the thickness of the overlying layer is sufficiently substantial. Arusoaie [23] examines the spatial and temporal properties of solutions to the initial boundary value problem associated with the linear theory of thermoelastic materials exhibiting a double porosity structure. We examine two appropriate time-weighted integral measures and develop exponential estimates that define the spatial characteristics of solutions. Rana *et al.* [24] performed a study on the vibrational characteristics of a hollow cylinder composed of a homogeneous and isotropic elastic material exhibiting double porosity. The study focuses on the impact of a magnetic field on the cylinder's behavior, particularly with nonlocal elasticity. Kumar and Vohra [25] investigated the vibration behavior of a microbeam with a twofold porosity structure (TDP), which is both homogenous and isotropic. This vibration is caused by pulsed laser heating. The study is conducted within the L-S's theory of thermoelasticity, which includes one relaxation time. Seema and Singhal [26,27] explored how wave propagation affects SAW macro- and nanosensors. Thus, shear horizontal (SH) waves are studied in an orthotropic piezoelectric quasicrystal (PQC) layer above an elastic framework (Model I), a piezoelectric substrate, and an orthotropic PQC substrate (Model II) using surface piezoelectricity theory. Previous research on surface acoustic wave sensors found significant restrictions in piezoelectric material selection and wave propagation orientation [28]. They study how wave propagation direction affects SAW macro and nanosensor efficacy to overcome technical barriers. A model is proposed to examine SH and anti-plane SH wave propagation in piezoelectric materials, considering surface effects. Seema and Singhal [26,29] discussed the potential applications of our findings in advanced engineering fields, such as geothermal energy extraction, oil recovery, and biomedical devices. It also highlighted the need for further experimental validation and the development of more efficient computational models for complex porous materials [30]. This study investigates the dynamics of hybrid nanofluids under electromagnetic fields, providing valuable insights into the coupling of thermal, mechanical, and electromagnetic effects. The techniques used in this work, such as the modeling of coupled fields and the use of numerical methods, are highly relevant to our study [31]. This work explores the reflection of hygrothermal waves in nonlocal thermoelastic materials, which aligns with our focus on wave propagation in double-porosity materials. The use of nonlocal theories and coupled thermoelastic models in this study provides a strong theoretical foundation for our work.

This work examines the equations governing the behavior of a thermoelastic material with a double-porosity structure and one relaxation time, in the presence of a magnetic field. The graphical representation illustrates the impact of the thermoelastic coupling parameter,

thermoelectric coupling parameter, and influence of the magnetic field on physical quantities with photo-thermoelastic effect and double porosity. The integration of double porosity and magneto-thermoelasticity is a novel approach, potentially opening doors to enhanced designs for semiconductors and porous materials. The integration of magnetic fields, dual porosity, and L-S thermoelasticity in a single model provides a new, more accurate approach to understanding material behavior in complex systems. The study's predictive power, ability to model real-world material behavior, and applicability to advanced materials for semiconductor and nanotechnology offer significant advantages for both scientific research and industrial applications. This is especially valuable for cutting-edge technologies in energy, sensors, and material optimization.

2 Formulation of the problem and basic equations

Suppose a homogeneous photo-thermoelastic half-space with a double-porosity structure in the undeformed state at reference temperature T_0 under the effect of Lorentz force F_i. It is clear that from the geometry of the problem (Figure 1), all physical functions will depend on (x, z, t) and how we obtain the displacement vector $\vec{u}$ as $\vec{u} = (u_1, 0, u_3)$. Consider a magnetic field with constant intensity $\vec{H} = (0, H_0, 0)$ in the y-axis direction. This results from an induced magnetic field $h = -H_0 e$ and an induced electric field $\vec{E}$ [32,33]:

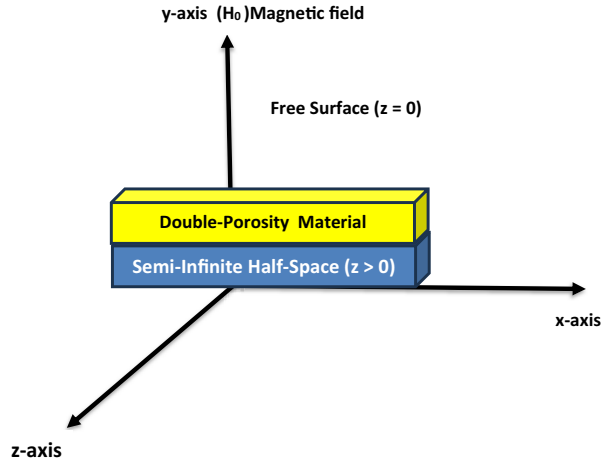

Figure 1: Geometry of the problem.

$$\text{curl } \vec{h} = \vec{J} + \varepsilon_0 \frac{\partial \vec{E}}{\partial t}, \tag{1}$$

$$\text{curl } \vec{E} = -\mu_0 \frac{\partial \vec{h}}{\partial t}, \tag{2}$$

$$\text{div } \vec{h} = 0, \tag{3}$$

$$\vec{E} = -\mu_0 \left(\frac{\partial \vec{u}}{\partial t} \times \vec{H} \right), \tag{4}$$

where μ_0 (H/m (N/A^2)) is the magnetic permeability for the free space, ε_0 (F/m (C^2/(N m^2))) is the electric permeability for the free space, and J (A/m^2) is the current density vector.

The equations and relations that describe the behavior of a thermoelastic solid with a double-porosity structure, which is both homogenous and isotropic, in the presence of a magnetic field and without any additional forces or heat sources, are provided by the L-S model:

Stress equation [1,6,34]:

$$t_{ij} = 2\mu e_{ij} + (\lambda e + b\Phi + d\Psi - \gamma T - \delta_n N)\delta_{ij}. \tag{5}$$

Equations for double porosity [35]:

$$\sigma_i = a\Phi_{,i} + b_1 \Psi_{,i}, \tag{6}$$

$$\tau_i = b_1 \Phi_{,i} + \gamma \Psi_{,i}. \tag{7}$$

Equations of motion [1,6,35]:

$$\mu \nabla^2 u_1 + (\lambda + \mu)\frac{\partial e}{\partial x} + b\frac{\partial \Phi}{\partial x} + d\frac{\partial \Psi}{\partial x} - \gamma \frac{\partial T}{\partial x} + \mu_0 H_0^2 \frac{\partial e}{\partial x} - \varepsilon_0 \mu_0^2 H_0^2 \ddot{u}_1 - \delta_n \frac{\partial N}{\partial x} = \rho \ddot{u}_1, \tag{8}$$

$$\mu \nabla^2 u_3 + (\lambda + \mu)\frac{\partial e}{\partial z} + b\frac{\partial \Phi}{\partial z} + d\frac{\partial \Psi}{\partial z} - \gamma \frac{\partial T}{\partial z} + \mu_0 H_0^2 \frac{\partial e}{\partial z} - \varepsilon_0 \mu_0^2 H_0^2 \ddot{u}_3 - \delta_n \frac{\partial N}{\partial z} = \rho \ddot{u}_3. \tag{9}$$

Equilibrated stress equations of motion [35]:

$$a\nabla^2 \Phi + b_1 \nabla^2 \Psi - be - \alpha_1 \Phi - \alpha_3 \Psi + \gamma_1 T = K_1 \ddot{\Phi}, \tag{10}$$

$$b_1 \nabla^2 \Phi + \gamma \nabla^2 \Psi - de - \alpha_3 \Phi - \alpha_2 \Psi + \gamma_2 T = K_2 \ddot{\Psi}. \tag{11}$$

Equations of heat [35,36]:

$$K^* \nabla^2 T = \left(1 + \tau_0 \frac{\partial}{\partial t}\right)(\rho c^* \dot{T} + \gamma_1 T_0 \dot{\phi} + \gamma_2 T_0 \dot{\psi} + \gamma T_0 \dot{e}) - \frac{E_g}{\tau} N, \tag{12}$$

$$D_E \nabla^2 N - \frac{N}{\tau} + \kappa T = \frac{\partial N}{\partial t}. \tag{13}$$

For simplicity, we introduce the following dimensionless variables [37,38]:

$(x', z') = \frac{\omega_1}{c_1}(x, z)$, $(u_1', u_3') = \frac{\omega_1}{c_1}(u_1, u_3)$, $\{\sigma_1', \tau_1'\} = \frac{c_1}{a\omega_1}\{\sigma_1, \tau_1\}$, $(t', \tau_0') = \omega_1(t, \tau_0)$, $[\Phi', \Psi'] = \frac{K_1\omega_1^2}{a_1}[\Phi, \Psi]$, $c_1^2 = \frac{\lambda + 2\mu}{\rho}$, $\gamma = (3\lambda + 2\mu)\alpha_t$, $\omega_1 = \frac{\rho c^* c_1^2}{K^*}$, $\nabla^2 = \frac{\omega_1^2}{c_1^2}\nabla'^2$, $T' = \frac{T}{T_0}$, $h' = \frac{h}{H_0}$, $t_{ij}' = \left(\frac{1}{\mu}\right)t_{ij}$, $(N', T') = \left(\frac{\delta_n N, \gamma T}{\lambda + 2\mu}\right)$.

Using the above dimensionless quantities, Eqs. (8)–(13) become

$$a_1\frac{\partial e}{\partial x} + a_2\nabla^2 u_1 + a_3\frac{\partial \Phi}{\partial x} + a_4\frac{\partial \Psi}{\partial x} - \frac{\partial T}{\partial x} - \frac{\partial N}{\partial x} = a_5\ddot{u}_1, \tag{14}$$

$$a_1\frac{\partial e}{\partial z} + a_2\nabla^2 u_3 + a_3\frac{\partial \Phi}{\partial z} + a_4\frac{\partial \Psi}{\partial z} - \frac{\partial T}{\partial z} - \frac{\partial N}{\partial z} = a_5\ddot{u}_3, \tag{15}$$

$$a_6\nabla^2\Phi + a_7\nabla^2\Psi - a_8 e - a_9\Phi - a_{10}\Psi + a_{11}T = \ddot{\Phi}, \tag{16}$$

$$a_{12}\nabla^2\Phi + a_{13}\nabla^2\Psi - a_{14}e - a_{15}\Phi - a_{16}\Psi + a_{17}T = \ddot{\Psi}, \tag{17}$$

$$\nabla^2 T - \left(1 + \tau_0\frac{\partial}{\partial t}\right)(\dot{T} + a_{18}\dot{\phi} + a_{19}\dot{\psi} + \varepsilon_1\dot{e}) - \varepsilon_2 N = 0, \tag{18}$$

$$\left(\nabla^2 - a_{20} - a_{21}\frac{\partial}{\partial t}\right)N + \varepsilon_3 T = 0. \tag{19}$$

The stress components can be expressed in dimensionless variables in the following manner:

$$\tau_{xx} = a_{22}e + a_{23}\frac{\partial u_1}{\partial x} - T - N + a_{24}\Phi + a_{25}\psi, \tag{20}$$

$$\tau_{zz} = a_{22}e + a_{23}\frac{\partial u_3}{\partial z} - T - N + a_{24}\Phi + a_{25}\psi, \tag{21}$$

$$\tau_{xz} = a_{23}e_{xz}, \tag{22}$$

where $a_1 = \frac{\mu + \lambda + \mu_0 H_0^2}{\rho c_1^2}$, $a_2 = \frac{\mu}{\rho c_1^2}$, $a_3 = \frac{ba_1}{\rho c_1^2 K_1\omega_1^2}$, $a_4 = \frac{da_1}{\rho c_1^2 K_1\omega_1^2}$, $a_5 = \frac{\varepsilon_0\mu_0^2 H_0^2}{\rho} + 1$, $a_6 = \frac{a}{c_1^2 K_1}$, $a_7 = \frac{b_1}{c_1^2 K_1}$, $a_8 = \frac{b}{a_1}$, $a_9 = \frac{a_1}{K_1 w_1^2}$, $a_{10} = \frac{a_3}{K_1\omega_1^2}$, $a_{11} = \frac{\gamma_1 T_0}{a_1}$, $a_{12} = \frac{b_1}{c_1^2 K_2}$, $a_{13} = \frac{\gamma}{c_1^2 K_2}$, $a_{14} = \frac{dK_1}{a_1 K_2}$, $a_{15} = \frac{a_3}{\omega_1^2 K_2}$, $a_{16} = \frac{a_2}{\omega_1^2 K_2}$, $a_{17} = \frac{\gamma_2 T_0 K_1}{a_1 K_2}$, $a_{18} = \frac{\gamma\,\gamma_1 T_0 a_1}{\rho K^* \omega_1^3}$, $a_{19} = \frac{\gamma\,\gamma_2 T_0 a_1}{\rho K^* \omega_1^3}$, $a_{20} = \frac{K^* t^*}{D_E \rho c^*}$, $a_{21} = \frac{K^*}{D_E \rho c^*}$, $a_{22} = \frac{\lambda}{\gamma T_0}$, $a_{23} = \frac{2\mu}{\gamma T_0}$, $a_{24} = \frac{ba_1}{K_1\omega_1^2\gamma T_0}$, $a_{25} = \frac{da_1}{K_1\omega_1^2\gamma T_0}$, $\varepsilon_1 = \frac{\gamma^2 T_0}{K^*\rho\omega_1}$, $\varepsilon_2 = \frac{a_T E_g}{d_n\rho\tau c^*\omega_1}$, $\varepsilon_3 = \frac{d_n K^* \kappa}{a_T \rho c^* D_E \omega_1}$, $\delta_n = (2\mu + 3\lambda)d_n$.

We define the displacement potentials ϕ_1 and ψ_1, which are related to the displacement components u_1 and u_3 as [39]

$$u_1 = \phi_{1,x} - \psi_{1,z}, \ldots u_3 = \phi_{1,z} + \psi_{1,x}. \tag{23}$$

Using Eq. (23) in Eqs. (14)–(18), we obtain

$$\left((a_1 + a_2)\nabla^2 - a_5\frac{\partial^2}{\partial t^2}\right)\phi_1 + a_3\Phi + a_4\Psi - T - N = 0, \tag{24}$$

$$\left(a_2\nabla^2 - a_5\frac{\partial^2}{\partial t^2}\right)\psi_1 = 0, \tag{25}$$

$$a_6\nabla^2\Phi + a_7\nabla^2\Psi - a_8\nabla^2\phi_1 - a_9\Phi - a_{10}\Psi + a_{11}T = \ddot{\Phi}, \tag{26}$$

$$a_{12}\nabla^2\Phi + a_{13}\nabla^2\Psi - a_{14}\nabla^2\phi_1 - a_{15}\Phi - a_{16}\Psi + a_{17}T = \ddot{\Psi}, \tag{27}$$

$$\nabla^2 T - \left(1 + \tau_0\frac{\partial}{\partial t}\right)(\dot{T} + a_{18}\dot{\phi} + a_{19}\dot{\psi} + \varepsilon_1\nabla^2\dot{\phi}_1) - \varepsilon_2 N = 0. \tag{28}$$

3 Normal mode analysis

The solution of the given physical variable can be expressed as the decomposition in terms of normal modes (derived by assuming exponential representations), as follows [40,41]:

$$[u_1,\ u_3,\ e,\ T,\ \phi_1,\ \psi_1, \Phi, \psi,\ \tau_{ij},\ N](x, z, t) = (u_1^*,\ u_3^*,\ e^*,\ T^*,\ \phi_1^*,\ \psi_1^*,\ \Phi^*,\ \psi^*,\ \tau_{ij}^*,\ N^*)(z)e^{(\omega t + iax)}, \tag{29}$$

where i is the imaginary unit, ω is the complex time constant (frequency), and a is the wave number in the x-direction.

Using (29) in Eqs. (19)–(22) and Eqs. (24)–(28) we obtain

$$(g_1 D^2 - g_2)\phi_1^* + a_3\Phi^* + a_4\Psi^* - T^* - N^* = 0, \tag{30}$$

$$(a_2 D^2 - g_3)\psi_1^* = 0, \tag{31}$$

$$(a_6 D^2 - g_4)\Phi^* + (a_7 D^2 - g_5)\Psi^* - (a_8 D^2 - g_6)\phi_1^* + a_{11}T^* = 0, \tag{32}$$

$$(a_{12} D^2 - g_7)\Phi^* + (a_{13} D^2 - g_8)\Psi^* - (a_{14} D^2 - g_9)\phi_1^* + a_{17}T^* = 0, \tag{33}$$

$$(D^2 - g_{10})T^* - g_{11}\phi^* - g_{12}\psi^* - (g_{13} D^2 - g_{14})\phi_1^* + g_{15}N^* = 0, \tag{34}$$

$$(D^2 - g_{16})N^* + \varepsilon_3 T^* = 0, \tag{35}$$

where $D = \frac{d}{dz}$, $g_1 = a_1 + a_2$, $g_2 = (g_1 a^2 + a_5\omega^2)$, $g_3 = a_2 a^2 + a_5\omega^2$, $g_4 = a_6 a^2 + a_9 + \omega^2$, $g_5 = a_7 a^2 + a_{10}$, $g_6 = a_8 a^2$, $g_7 = a_{12}a^2 + a_{15}$, $g_8 = a_{13}a^2 + a_{16} + \omega^2$, $g_9 = a_{14}a^2$, $g_{10} = a^2 + (1 + \tau_0\omega)\omega$, $g_{11} = a_{18}\omega(1 + \tau_0\omega)$, $g_{12} = a_{19}\omega(1 + \tau_0\omega)$, $g_{13} = \varepsilon_1\omega(1 + \tau_0\omega)$, $g_{14} = a^2 g_{13}$, $g_{15} = -\varepsilon_2$, $g_{16} = a^2 + a_{20} + a_{21}\omega$.

Eliminating T^*, N^*, ϕ_1^*, ϕ^*, and ψ^* in Eqs. (30), (32), (33), (34), and (35) yields

$$(D^{10} - \Delta_1 D^8 + \Delta_2 D^6 - \Delta_3 D^4 + \Delta_4 D^2 - \Delta_5)\{T^*,\ N^*, \phi_1^*,\ \phi^*,\ \psi^*\}(z)e^{(\omega t + iax)} = 0, \tag{36}$$

where

$$\Delta_1 = \frac{-1}{(a_{13}a_6g_1 - a_{12}a_7g_1)}\begin{Bmatrix} a_{14}a_4a_6 - a_{14}a_3a_7 + a_{13}a_3a_8 - a_{12}a_4a_8 - a_{13}a_6g_1g_{10} + a_{12}a_7g_1g_{10} - a_{13}a_6g_{13} + a_{12}a_7g_{13} \\ - a_{13}a_6g_1g_{16} + a_{12}a_7g_1g_{16} - a_{13}a_6g_2 + a_{12}a_7g_2 - a_{13}g_1g_4 + a_{12}g_1g_5 + a_7g_1g_7 - a_6g_1g_8 \end{Bmatrix}, \tag{37}$$

$$\Delta_2 = \frac{1}{(a_{13}a_6g_1 - a_{12}a_7g_1)}\begin{Bmatrix} - a_{14}a_4a_6g_{10} + a_{14}a_3a_7g_{10} - a_{13}a_3a_8g_{10} + a_{12}a_4a_8g_{10} + a_{14}a_7g_{11} - a_{13}a_8g_{11} + a_{11}a_{13}g_1g_{11} \\ - a_{17}a_7g_1g_{11} - a_{14}a_6g_{12} + a_{12}a_8g_{12} - a_{11}a_{12}g_1g_{12} + a_{17}a_6g_1g_{12} - a_{11}a_{13}a_3g_{13} + a_{11}a_{12}a_4g_{13} \\ - a_{17}a_4a_6g_{13} + a_{17}a_3a_7g_{13} + a_{13}a_6g_{14} - a_{12}a_7g_{14} - a_{14}a_4a_6g_{16} + a_{14}a_3a_7g_{16} - a_{13}a_3a_8g_{16} \\ + a_{12}a_4a_8g_{16} + a_{13}a_6g_1g_{10}g_{16} - a_{12}a_7g_1g_{10}g_{16} + a_{13}a_6g_{13}g_{16} - a_{12}a_7g_{13}g_{16} + a_{13}a_6g_{10}g_2 - a_{12}a_7g_{10}g_2 \\ + a_{13}a_6g_{16}g_2 - a_{12}a_7g_{16}g_2 - a_{14}a_4g_4 + a_{13}g_1g_{10}g_4 + a_{13}g_{13}g_4 + a_{13}g_1g_{16}g_4 + a_{13}g_2g_4 + a_{14}a_3g_5 \\ - a_{12}g_1g_{10}g_5 - a_{12}g_{13}g_5 - a_{12}g_1g_{16}g_5 - a_{12}g_2g_5 - a_{13}a_3g_6 + a_{12}a_4g_6 + a_4a_8g_7 - a_7g_1g_{10}g_7 - a_7g_{13}g_7 \\ - a_7g_1g_{16}g_7 - a_7g_2g_7 - g_1g_5g_7 - a_3a_8g_8 + a_6g_1g_{10}g_8 + a_6g_{13}g_8 + a_6g_1g_{16}g_8 + a_6g_2g_8 + g_1g_4g_8 \\ - a_4a_6g_9 + a_3a_7g_9 + a_{13}a_6g_{13}\varepsilon_3 - a_{12}a_7g_{13}\varepsilon_3 - a_{13}a_6g_1g_{15}\varepsilon_3 + a_{12}a_7g_1g_{15}\varepsilon_3 \end{Bmatrix} \tag{38}$$

$$\Delta_3 = \frac{-1}{(a_{13}a_6g_1 - a_{12}a_7g_1)}\begin{Bmatrix} a_{11}a_{14}a_4g_{11} - a_{17}a_4a_8g_{11} - a_{11}a_{14}a_3g_{12} + a_{17}a_3a_8g_{12} + a_{11}a_{13}a_3g_{14} \\ - a_{11}a_{12}a_4g_{14} + a_{17}a_4a_6g_{14} - a_{17}a_3a_7g_{14} + a_{14}a_4a_6g_{10}g_{16} - a_{14}a_3a_7g_{10}g_{16} + a_{13}a_3a_8g_{10}g_{16} \\ - a_{12}a_4a_8g_{10}g_{16} - a_{14}a_7g_{11}g_{16} + a_{13}a_8g_{11}g_{16} - a_{11}a_{13}g_1g_{11}g_{16} + a_{17}a_7g_1g_{11}g_{16} + a_{14}a_6g_{12}g_{16} - a_{12}a_8g_{12}g_{16} \\ + a_{11}a_{12}g_1g_{12}g_{16} - a_{17}a_6g_1g_{12}g_{16} + a_{11}a_{13}a_3g_{13}g_{16} - a_{11}a_{12}a_4g_{13}g_{16} + a_{17}a_4a_6g_{13}g_{16} - a_{17}a_3a_7g_{13}g_{16} \\ - a_{13}a_6g_{14}g_{16} + a_{12}a_7g_{14}g_{16} - a_{11}a_{13}g_{11}g_2 + a_{17}a_7g_{11}g_2 + a_{11}a_{12}g_{12}g_2 - a_{17}a_6g_{12}g_2 - a_{13}a_6g_{10}g_{16}g_2 \\ + a_{12}a_7g_{10}g_{16}g_2 + a_{14}a_4g_{10}g_4 + a_{14}g_{12}g_4 - a_{17}g_1g_{12}g_4 + a_{17}a_4g_{13}g_4 - a_{13}g_{14}g_4 + a_{14}a_4g_{16}g_4 \\ - a_{13}g_1g_{10}g_{16}g_4 - a_{13}g_{13}g_{16}g_4 - a_{13}g_{10}g_2g_4 - a_{13}g_{16}g_2g_4 - a_{14}a_3g_{10}g_5 - a_{14}g_{11}g_5 + a_{17}g_1g_{11}g_5 \\ - a_{17}a_3g_{13}g_5 + a_{12}g_{14}g_5 - a_{14}a_3g_{16}g_5 + a_{12}g_1g_{10}g_{16}g_5 + a_{12}g_{13}g_{16}g_5 + a_{12}g_{10}g_2g_5 \\ + a_{12}g_{16}g_2g_5 + a_{13}a_3g_{10}g_6 - a_{12}a_4g_{10}g_6 + a_{13}g_{11}g_6 - a_{12}g_{12}g_6 + a_{13}a_3g_{16}g_6 - a_{12}a_4g_{16}g_6 \\ - a_4a_8g_{10}g_7 - a_8g_{12}g_7 - a_{11}a_4g_{13}g_7 + a_7g_{14}g_7 - a_4a_8g_{16}g_7 + a_7g_1g_{10}g_{16}g_7 + a_7g_{13}g_{16}g_7 \\ + a_7g_{10}g_2g_7 + a_7g_{16}g_2g_7 + g_1g_{10}g_5g_7 + g_{13}g_5g_7 + g_1g_{16}g_5g_7 + +a_{11}g_1g_{12}g_7g_2g_5g_7 - a_4g_6g_7 \\ + a_3a_8g_{10}g_8 + a_8g_{11}g_8 - a_{11}g_1g_{11}g_8 + a_{11}a_3g_{13}g_8 - a_6g_{14}g_8 + a_3a_8g_{16}g_8 - a_6g_1g_{10}g_{16}g_8 \\ - a_6g_{13}g_{16}g_8 - a_6g_{10}g_2g_8 - a_6g_{16}g_2g_8 - g_1g_{10}g_4g_8 - g_{13}g_4g_8 - g_1g_{16}g_4g_8 - g_2g_4g_8 + a_3g_6g_8 \\ + a_4a_6g_{10}g_9 - a_3a_7g_{10}g_9 - a_7g_{11}g_9 + a_6g_{12}g_9 + a_4a_6g_{16}g_9 - a_3a_7g_{16}g_9 + a_{13}a_8g_{11}\varepsilon_3 + a_4g_4g_9 \\ - a_3g_5g_9 - a_{14}a_7g_{11}\varepsilon_3 - a_{14}a_4a_6g_{15}\varepsilon_3 + a_{14}a_6g_{12}\varepsilon_3 - a_{12}a_8g_{12}\varepsilon_3 - a_{13}a_6g_{14}\varepsilon_3 \\ + a_{12}a_7g_{14}\varepsilon_3 + a_{14}a_3a_7g_{15}\varepsilon_3 - a_{13}a_3a_8g_{15}\varepsilon_3 + a_{12}a_4a_8g_{15}\varepsilon_3 + a_{13}a_6g_{15}g_2\varepsilon_3 \\ - a_{12}a_7g_{15}g_2\varepsilon_3 - a_{13}g_{13}g_4\varepsilon_3 + a_{13}g_1g_{15}g_4\varepsilon_3 + a_{12}g_{13}g_5\varepsilon_3 - a_{12}g_1g_{15}g_5\varepsilon_3 + a_7g_{13}g_7\varepsilon_3 \\ - a_7g_1g_{15}g_7\varepsilon_3 - a_6g_{13}g_8\varepsilon_3 + a_6g_1g_{15}g_8\varepsilon_3 \end{Bmatrix} \tag{39}$$

$$\Delta_4 = \frac{1}{(a_{13}a_6g_1 - a_{12}a_7g_1)}\begin{Bmatrix} -a_{11}a_{14}a_4g_{11}g_{16} + a_{17}a_4a_8g_{11}g_{16} + a_{11}a_{14}a_3g_{12}g_{16} - a_{17}a_3a_8g_{12}g_{16} - a_{11}a_{13}a_3g_{14}g_{16} \\ + a_{11}a_{12}a_4g_{14}g_{16} - a_{17}a_4a_6g_{14}g_{16} + a_{17}a_3a_7g_{14}g_{16} + a_{11}a_{13}g_{11}g_{16}g_2 - a_{17}a_7g_{11}g_{16}g_2 \\ - a_{11}a_{12}g_{12}g_{16}g_2 + a_{17}a_6g_{12}g_{16}g_2 - a_{17}a_4g_{14}g_4 - a_{14}a_4g_{10}g_{16}g_4 - a_{14}g_{12}g_{16}g_4 \\ + a_{17}g_1g_{12}g_{16}g_4 - a_{17}a_4g_{13}g_{16}g_4 + a_{13}g_{14}g_{16}g_4 + a_{17}g_{12}g_2g_4 + a_{13}g_{10}g_{16}g_2g_4 \\ + a_{17}a_3g_{14}g_5 + a_{14}a_3g_{10}g_{16}g_5 + a_{14}g_{11}g_{16}g_5 - a_{17}g_1g_{11}g_{16}g_5 + a_{17}a_3g_{13}g_{16}g_5 - a_{12}g_{14}g_{16}g_5 \\ - a_{17}g_{11}g_2g_5 - a_{12}g_{10}g_{16}g_2g_5 + a_{17}a_4g_{11}g_6 - a_{17}a_3g_{12}g_6 - a_{13}a_3g_{10}g_{16}g_6 + a_{12}a_4g_{10}g_{16}g_6 \\ - a_{13}g_{11}g_{16}g_6 + a_{12}g_{12}g_{16}g_6 + a_{11}a_4g_{14}g_7 + a_4a_8g_{10}g_{16}g_7 + a_8g_{12}g_{16}g_7 - a_{11}g_1g_{12}g_{16}g_7 \\ + a_{11}a_4g_{13}g_{16}g_7 - a_7g_{14}g_{16}g_7 - a_{11}g_{12}g_2g_7 - a_7g_{10}g_{16}g_2g_7 - g_{14}g_5g_7 - g_1g_{10}g_{16}g_5g_7 \\ - g_{13}g_{16}g_5g_7 - g_{10}g_2g_5g_7 - g_{16}g_2g_5g_7 + a_4g_{10}g_6g_7 + g_{12}g_6g_7 + a_4g_{16}g_6g_7 \\ - a_{11}a_3g_{14}g_8 - a_3a_8g_{10}g_{16}g_8 - a_8g_{11}g_{16}g_8 + a_{11}g_1g_{11}g_{16}g_8 - a_{11}a_3g_{13}g_{16}g_8 + a_6g_{14}g_{16}g_8 \\ + a_{11}g_{11}g_2g_8 + a_6g_{10}g_{16}g_2g_8 + g_{14}g_4g_8 + g_1g_{10}g_{16}g_4g_8 + g_{13}g_{16}g_4g_8 + g_{10}g_2g_4g_8 + g_{16}g_2g_4g_8 \\ - a_3g_{10}g_6g_8 - g_{11}g_6g_8 - a_3g_{16}g_6g_8 - a_{11}a_4g_{11}g_9 + a_{11}a_3g_{12}g_9 - a_4a_6g_{10}g_{16}g_9 \\ + a_3a_7g_{10}g_{16}g_9 + a_7g_{11}g_{16}g_9 - a_6g_{12}g_{16}g_9 - a_4g_{10}g_4g_9 - g_{12}g_4g_9 - a_4g_{16}g_4g_9 \\ + a_3g_{10}g_5g_9 + g_{11}g_5g_9 + a_3g_{16}g_5g_9 - a_{14}g_{12}g_4\varepsilon_3 + a_{13}g_{14}g_4\varepsilon_3 + a_{14}a_4g_{15}g_4\varepsilon_3 \\ - a_{13}g_{15}g_2g_4\varepsilon_3 + a_{14}g_{11}g_5\varepsilon_3 - a_{12}g_{14}g_5\varepsilon_3 - a_{14}a_3g_{15}g_5\varepsilon_3 + a_{12}g_{15}g_2g_5\varepsilon_3 - a_{13}g_{11}g_6\varepsilon_3 \\ + a_{12}g_{12}g_6\varepsilon_3 + a_{13}a_3g_{15}g_6\varepsilon_3 - a_{12}a_4g_{15}g_6\varepsilon_3 + a_8g_{12}g_7\varepsilon_3 - a_7g_{14}g_7\varepsilon_3 - a_4a_8g_{15}g_7\varepsilon_3 + a_7g_{15}g_2g_7\varepsilon_3 \\ - g_{13}g_5g_7\varepsilon_3 + g_1g_{15}g_5g_7\varepsilon_3 - a_8g_{11}g_8\varepsilon_3 + a_6g_{14}g_8\varepsilon_3 + a_3a_8g_{15}g_8\varepsilon_3 - a_6g_{15}g_2g_8\varepsilon_3 + g_{13}g_4g_8\varepsilon_3 \\ - g_1g_{15}g_4g_8\varepsilon_3 + a_7g_{11}g_9\varepsilon_3 - a_6g_{12}g_9\varepsilon_3 + a_4a_6g_{15}g_9\varepsilon_3 - a_3a_7g_{15}g_9\varepsilon_3 \end{Bmatrix} \tag{40}$$

$$\Delta_5 = \frac{-1}{(a_{13}a_6g_1 - a_{12}a_7g_1)}\begin{Bmatrix} a_{17}a_4g_{14}g_{16}g_4 - a_{17}g_{12}g_{16}g_2g_4 - a_{17}a_3g_{14}g_{16}g_5 + a_{17}g_{11}g_{16}g_2g_5 - a_{17}a_4g_{11}g_{16}g_6 + a_{17}a_3g_{12}g_{16}g_6 \\ - a_{11}a_4g_{14}g_{16}g_7 + a_{11}g_{12}g_{16}g_2g_7 + g_{14}g_{16}g_5g_7 + g_{10}g_{16}g_2g_5g_7 - a_4g_{10}g_{16}g_6g_7 - g_{12}g_{16}g_6g_7 \\ + a_{11}a_3g_{14}g_{16}g_8 - a_{11}g_{11}g_{16}g_2g_8 - g_{14}g_{16}g_4g_8 - g_{10}g_{16}g_2g_4g_8 + a_3g_{10}g_{16}g_6g_8 + g_{11}g_{16}g_6g_8 \\ + a_{11}a_4g_{11}g_{16}g_9 - a_{11}a_3g_{12}g_{16}g_9 + a_4g_{10}g_{16}g_4g_9 + g_{12}g_{16}g_4g_9 - a_3g_{10}g_{16}g_5g_9 - g_{11}g_{16}g_5g_9 \\ + g_{14}g_5g_7\varepsilon_3 - g_{15}g_2g_5g_7\varepsilon_3 - g_{12}g_6g_7\varepsilon_3 + a_4g_{15}g_6g_7\varepsilon_3 - g_{14}g_4g_8\varepsilon_3 + g_{15}g_2g_4g_8\varepsilon_3 + g_{11}g_6g_8\varepsilon_3 \\ - a_3g_{15}g_6g_8\varepsilon_3 + g_{12}g_4g_9\varepsilon_3 - a_4g_{15}g_4g_9\varepsilon_3 - g_{11}g_5g_9\varepsilon_3 + a_3g_{15}g_5g_9\varepsilon_3 \end{Bmatrix} \tag{41}$$

Technical factors were used to solve the main ordinary differential equation (ODE) (36) as follows:

$$(D^2 - m_1^2)(D^2 - m_2^2)(D^2 - m_3^2)(D^2 - m_4^2)(D^2 - m_5^2)\{T^*,\ N^*,\ \phi_1^*,\ \phi^*,\ \psi^*\}(z)e^{(\omega t + iax)} = 0, \tag{42}$$

where $m_i^2 (i = 1, 2, 3, 4, 5)$ represents the roots that they may take in the positive real part when $z \to \infty$. The solution of equation (ODE) (42) takes the following form (according to the linearity of the problem):

$$T^*(z, \omega, a) = \sum_{i=1}^{5} B_i(\omega, a)e^{-m_i z}. \tag{43}$$

In the same way, the solutions of the other quantities can be expressed as follows:

$$N^*(z, b, \omega) = \sum_{i=1}^{5} B_i'(a, \omega)e^{-m_i z} = \sum_{i=1}^{5} h_{1i}B_i(a, \omega)e^{-m_i z}, \tag{44}$$

$$\begin{aligned} \phi_1^*(z, b, \omega) &= \sum_{i=1}^{5} B_i''(b, \omega)\exp(-m_i z) \\ &= \sum_{i=1}^{3} h_{2i}B_i(b, \omega)\exp(-m_i z), \end{aligned} \tag{45}$$

$$\begin{aligned} \phi^*(z, a, \omega) &= \sum_{i=1}^{5} B_i'''(a, \omega)\exp(-m_i z) \\ &= \sum_{i=1}^{5} h_{3i}B_i(a, \omega)\exp(-m_i z), \end{aligned} \tag{46}$$

$$\begin{aligned} \psi^*(z, a, \omega) &= \sum_{i=1}^{5} B_i''''(a, \omega)\exp(-m_i z) \\ &= \sum_{i=1}^{5} h_{4i}B_i(a, \omega)\exp(-m_i z), \end{aligned} \tag{47}$$

$$\psi_1^*(z, a, \omega) = B_6(a, \omega)e^{-m_6 z}, \quad m_6 = \sqrt{\frac{g_3}{a_2}}. \tag{48}$$

Since

$$u_1^*(z) = ia\phi_1^* - D\psi_1^*, \tag{49}$$

$$u_3^*(z) = D\phi_1^* + ia\psi_1^*. \tag{50}$$

Then,

$$u_1^*(z) = ia\sum_{i=1}^{5} B_i''(b,\omega)\mathrm{e}^{-m_i z} + m_6 B_6(b,\omega)\exp(-m_6 z), \tag{51}$$

$$u_3^*(z) = -\sum_{i=1}^{5} m_i B_i''(b,\omega)\mathrm{e}^{-m_i z} + iaB_6(b,\omega)\exp(-m_6 z). \tag{52}$$

The stress components can be expressed using dimensionless variables. By substituting the stress displacement from Eqs. (51) and (52) into Eqs. (20)–(22), we obtain the components in the following form:

$$\tau_{xx}^* = \sum_{i=1}^{5} h_{5i} B_i \mathrm{e}^{-m_i z} + h_5 B_6 \mathrm{e}^{-m_6 z}, \tag{53}$$

$$\tau_{zz}^* = \sum_{i=1}^{5} h_{6i} B_i \mathrm{e}^{-m_i z} - h_5 B_6 \mathrm{e}^{-m_6 z}, \tag{54}$$

$$\tau_{xz}^* = \sum_{i=1}^{5} h_{7i} B_i \mathrm{e}^{-m_i z} + h_6 B_6 \mathrm{e}^{-m_6 z}. \tag{55}$$

The dimensionless variables for the components of σ_i and τ_i are

$$\sigma_3 = \eta_1 \Phi_{,z} + \eta_2 \Psi_{,z}, \tag{56}$$

$$\tau_3 = \eta_2 \Phi_{,z} + \eta_3 \Psi_{,z}, \tag{57}$$

where $\eta_1 = \frac{a_1}{k_1\omega_1^2}$, $\eta_2 = \frac{b_1 a_1}{a k_1 \omega_1^2}$, $\eta_3 = \frac{\gamma a_1}{a k_1 \omega_1^2}$.

To obtain the solution of σ_3 and τ_3, we substitute from Eqs. (46), (47) in (56) and (57), and obtain

$$\sigma_3^* = \sum_{i=1}^{5} h_{8i} B_i \mathrm{e}^{-k_i z}, \tag{58}$$

$$\tau_3^* = \sum_{i=1}^{5} h_{9i} B_i \mathrm{e}^{-m_i z}, \tag{59}$$

where B_6, $B_i, B_i', B_i'', B_i^{(3)}, B_i^{(4)}$, and $B_i^{(5)}$, $i = 1, 2, 3, 4, 5$, are unknown parameters depending on the parameter (a, ω). The relationship between the unknown parameters B_6, $B_i, B_i', B_i'', B_i^{(3)}, B_i^{(4)}$, and $B_i^{(5)}$, $i = 1, 2, 3, 4, 5$, can be obtained when using the main equations (Eqs. (21)–(26) and (27)), which take the following relationship:

$$h_{1i} = \frac{\varepsilon_3}{b_{16} - m_i^2},$$

$$h_{2i} = \frac{\left\{\begin{matrix} -\left((a_4(-b_4 + a_6 m_i^2) + a_3(b_5 - a_7 m_i^2))(a_4 a_{17} - (1 + h_{1i})(b_8 - a_{13} m_i^2)\right)\right) \\ +\left(a_4 a_{11} - (1 + h_{1i})(b_5 - a_7 m_i^2)\right)(a_4(-b_7 + a_{12} m_i^2) + a_3(b_8 - a_{13} m_i^2)) \end{matrix}\right\}}{\left\{\begin{matrix} (a_4(-b_7 + a_{12} m_i^2) + a_3(b_8 - a_{13} m_i^2))(a_4(b_6 - a_8 m_i^2) + (b_5 - a_7 m_i^2)(-b_2 + b_1 m_i^2)) \\ -(a_4(-b_4 + a_6 m_i^2) + a_3(b_5 - a_7 m_i^2))(a_4(b_9 - a_{14} m_i^2) + (b_8 - a_{13} m_i^2)(-b_2 + b_1 m_i^2)) \end{matrix}\right\}},$$

$$h_{3i} = \frac{\begin{matrix} \{(1 + h_{1i})(g_6 g_8 - g_5 g_9 + (a_{14} g_5 - a_{13} g_6 - a_8 a_6 + a_7 g_9) m_i^2 + (-a_{14} a_7 + a_{13} a_8) m_i^4) \\ +a_{17}(a4(-g_6 + a_8 m_i^2) + (g_5 - a_7 m_i^2)(g_2 - g_1 m_i^2)) + a_{11}(a_4(g_9 - a_{14} m_i^2) + (a_6 - a_{13} m_i^2)(-g_2 + g_1 m_i^2))\} \end{matrix}}{\left\{\begin{matrix} g_2 g_5 g_7 - a_4 g_6 g_7 - g_2 g_4 a_6 + a_3 g_6 a_6 + a_4 g_4 g_9 - a_3 g_5 g_9 + (-a_{14} a_4 g_4 + a_{13} g_2 g_4 + a_{14} a_3 g_5 - a_{12} g_2 g_5 \\ -a_{13} a_3 g_6 + a_{12} a_4 g_6 + a_4 a_8 g_7 - a_7 g_2 g_7 - g_1 g_5 g_7 - a_3 a_8 a_6 + a_6 g_2 a_6 + g_1 g_4 a_6 - a_4 a6 g_9 + a_3 a_7 g_9) m_i^2 \\ +\left(\begin{matrix} a_{14} a_4 a_6 - a_{14} a_3 a_7 + a_{13} a_3 a_8 - a_{12} a_4 a_8 - a_{13} a_6 g_2 + a_{12} a_7 g_2 - a_{13} g_1 g_4 \\ +a_{12} g_1 g_5 + a_7 g_1 g_7 - a_6 g_1 a_6 \end{matrix}\right) m_i^4 + (a_{13} a6 - a_{12} a_7) g_1 m_i^6) \end{matrix}\right\}},$$

$$h_{4i} = \frac{\begin{matrix} \left\{-((1 + h_{1i})(g_6 g_7 - g_4 g_9 + (a_{14} g_4 - a_{12} g_6 - a_8 g_7 + a_6 g_9) m_i^2 + - a_{14} a_6 + a_{12} a_8) m_i^4)) + a_{11}(-a_3 g_9 + a_{14} a_3 m_i^2 \right. \\ \left. + (g_7 - a_{12} m_i^2)(g_2 - g_1 m_i^2)) a_{17}(a_3(g_6 - a_8 m_i^2) + (g_4 - a_6 m_i^2)(-g_2 + g_1 m_i^2))\right\} \end{matrix}}{\left\{\begin{matrix} (g_2 g_5 g_7 - a_4 g_6 g_7 - g_2 g_4 a_6 + a_3 g_6 a_6 + a_4 g_4 g_9 - a_3 g_5 g_9 + (-a_{14} a_4 g_4 + a_{13} g_2 g_4 + a_{14} a_3 g_5 - a_{12} g_2 g_5 \\ -a_{13} a_3 g_6 + a_{12} a_4 g_6 + a_4 a_8 g_7 - a_7 g_2 g_7 - g_1 g_5 g_7 - a_3 a_8 g_8 + a_6 g_2 g_8 + g_1 g_4 g_8 - a_4 a_6 g_9 \\ +a_3 a_7 g_9) m_i^2 + (a_{14} a_4 a_6 - a_{14} a_3 a_7 + a_{13} a_3 a_8 - a_{12} a_4 a_8 - a_{13} a_6 g_2 + a_{12} a_7 g_2 - a_{13} g_1 g_4 \\ +a_{12} g_1 g_5 + a_7 g_1 g_7 - a_6 g_1 g_8) m_i^4 + (a_{13} a_6 - a_{12} a_7) g_1 m_i^6) \end{matrix}\right\}}$$

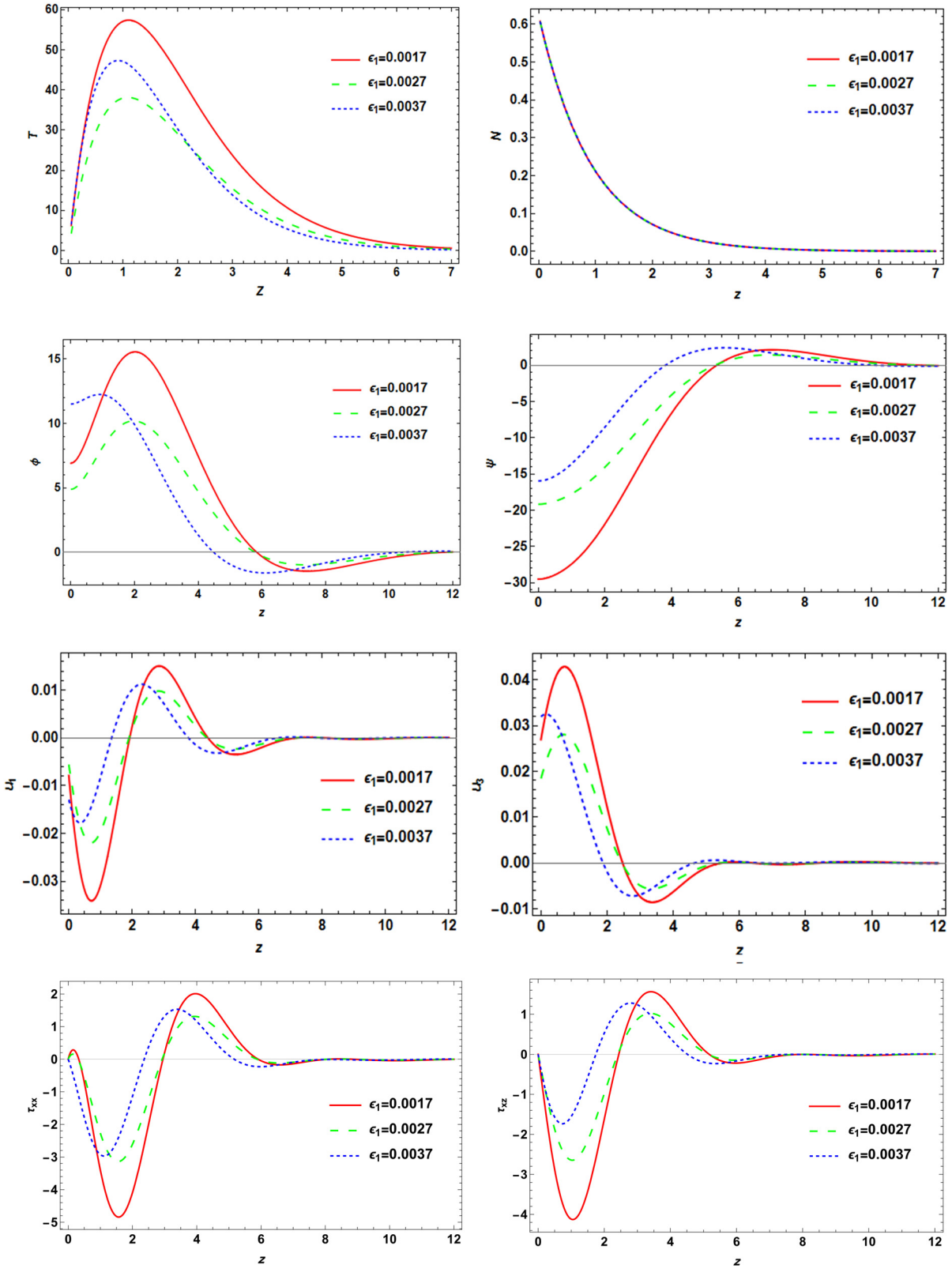

Figure 2: Variation of physical field distributions with distance at different thermoelastic coupling parameter ε_1 values when $\varepsilon_3 = -1.4 \times 10^{-35}$ under the effect of a magnetic field $H_0 = 10^5$ with double porosity.

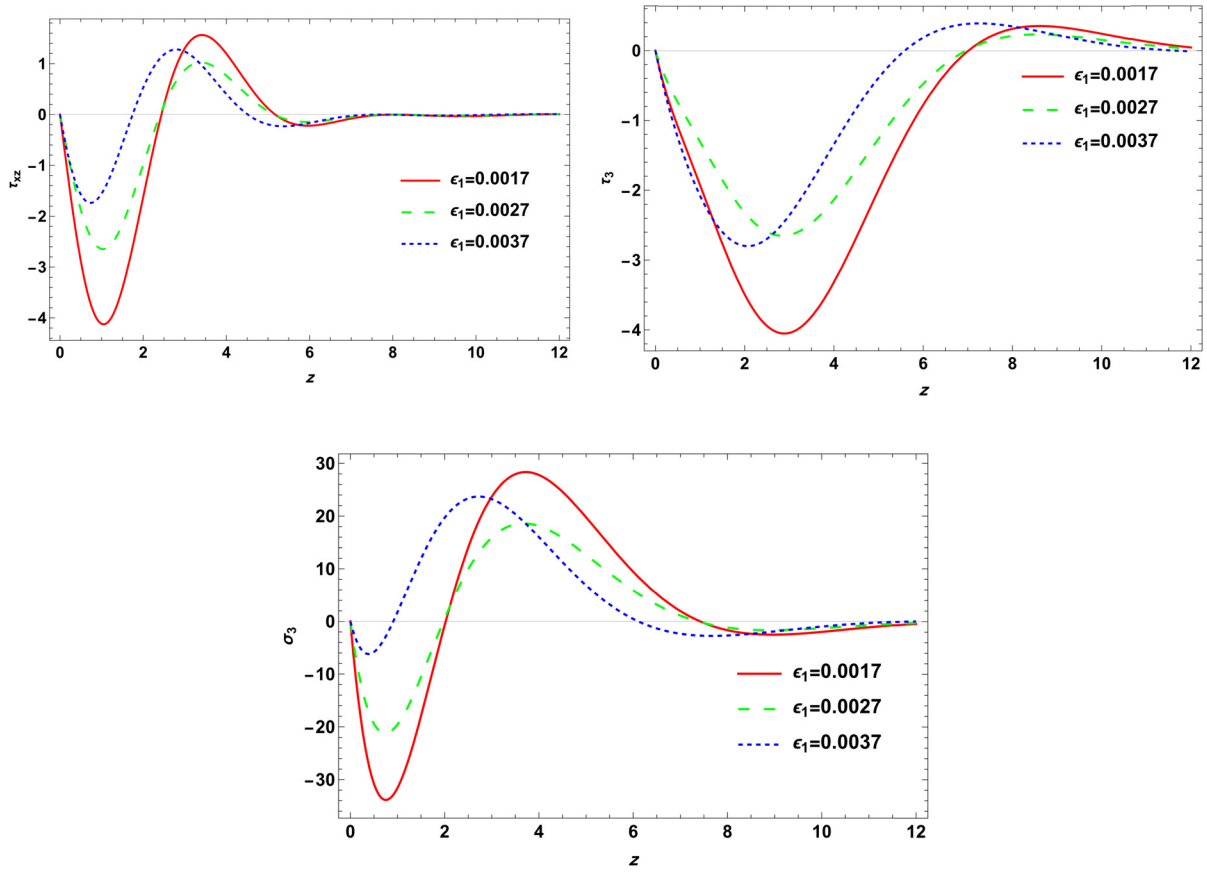

Figure 2: (*Continued*)

$h_{5i} = (a_{22}(m_i^2 - a^2) - a_{23}a^2)h_{2i} - 1 - h_{1i} + (a_{24})h_{3i} + (a_{25})h_{4i}$, $h_{6i} = [a_{22}(m_i^2 - a^2) + a_{23}m_i^2]h_{2i} - 1 - h_{1i} + (a_{24})h_{3i} + (a_{25})h_{4i}$, $h_5 = (iam_6a_{23})$, $h_6 = (-\frac{1}{2}a_{23}(m_6^2 + a^2))$, $h_{7i} = (-iam_ia_{23}h_{2i})$, $h_{8i} = (-\eta_1 m_i h_{3i} - \eta_2 m_i h_{4i})$, $h_{9i} = (-\eta_2 m_i h_{3i} - \eta_3 m_i h_{4i})$.

The solutions to the major variables that transform the domain in terms of unknown parameters $B_i(a, \omega)$ are given above. The parameters can be obtained from the following boundary conditions.

4 Boundary conditions

We apply six boundary conditions for the present problem at the plane surface $z = 0$:

$$\tau_{xx} = P_1 e^{(\omega t + iax)}, \tag{60}$$

$$\tau_{xz} = 0, \tag{61}$$

$$N = n_0 e^{(\omega t + iax)}, \tag{62}$$

$$\tau_3 = 0, \tag{63}$$

$$\sigma_3 = 0, \tag{64}$$

$$T = P_2 e^{(\omega t + iax)}. \tag{65}$$

Substituting Eqs. (60)–(65) in (43), (44), (53), (55), (56), and (57), we obtain

$$\sum_{i=1}^{5} h_{5i}B_i + h_5B_6 = P_1, \tag{66}$$

$$\sum_{i=1}^{5} h_{7i}B_i + h_6B_6 = 0, \tag{67}$$

$$\sum_{i=1}^{5} h_{1i}B_i = n_0, , \tag{68}$$

$$\sum_{i=1}^{5} h_{9i}B_i = 0, \tag{69}$$

$$\sum_{i=1}^{5} h_{8i}B_i = 0, \tag{70}$$

$$\sum_{i=1}^{5} B_i = P_2. \tag{71}$$

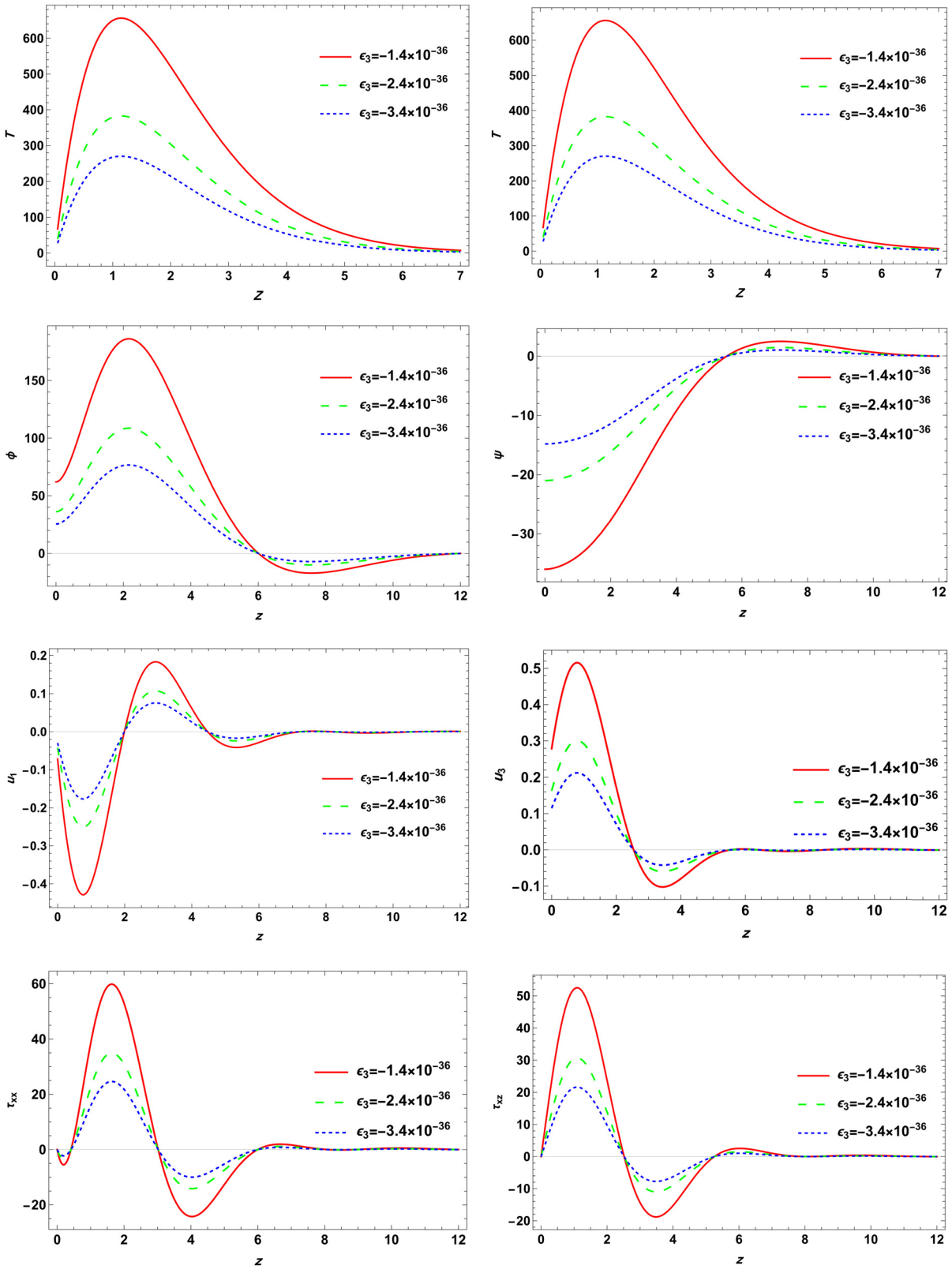

Figure 3: Variation in physical field distributions with distance at different thermoelectric ε_3 values when $\varepsilon_1 = 0.0017$ under the influence of a magnetic field and double porosity.

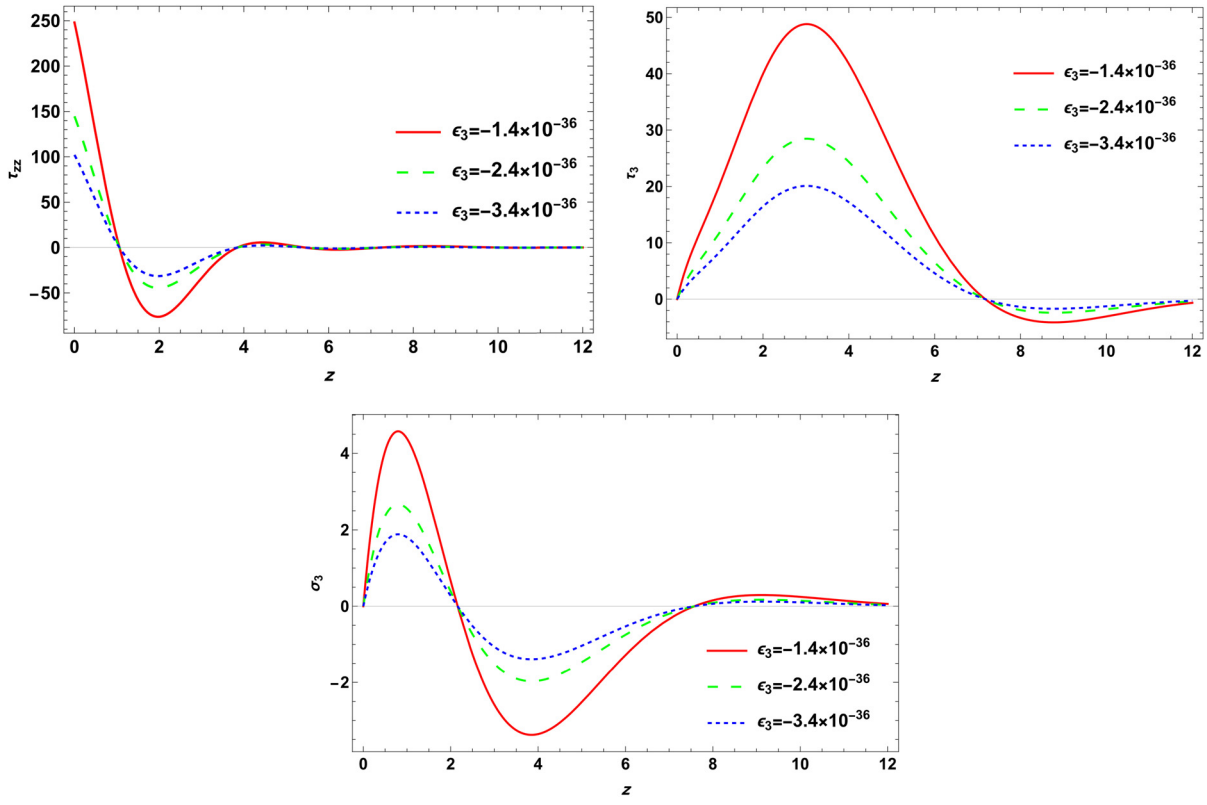

Figure 3: (*Continued*)

To obtain B_1, B_2, ..., B_5, B_6, we can substitute Eqs. (66)–(71) in the following matrix:

$$\begin{pmatrix} B_1 \\ B_2 \\ B_3 \\ B_4 \\ B_5 \\ B_6 \end{pmatrix} = \begin{pmatrix} h_{51} & h_{52} & h_{53} & h_{54} & h_{55} & h_5 \\ h_{71} & h_{72} & h_{73} & h_{74} & h_{75} & h_6 \\ h_{11} & h_{12} & h_{13} & h_{14} & h_{15} & 0 \\ h_{91} & h_{92} & h_{93} & h_{94} & h_{95} & 0 \\ h_{81} & h_{82} & h_{83} & h_{84} & h_{85} & 0 \\ 1 & 1 & 1 & 1 & 1 & 0 \end{pmatrix}^{-1} \cdot \begin{pmatrix} p_1 \\ 0 \\ n_0 \\ 0 \\ 0 \\ p_2 \end{pmatrix}. \quad (72)$$

5 Numerical results

The effect of a magnetic field on double porosity is now investigated, and numerical findings are presented. Silicon is chosen as the thermoelastic material, and the following values of physical constants are employed to attain this purpose [26,27].

$\lambda = 6.4 \times 10^{10}$ N m^{-2}, $\mu = 6.5 \times 10^{10}$ N m^{-2}, $K = 3.86 \times 10^3$ N s^{-1} K^{-1}, $c_1 = 2.5$ m/s, $\omega = -1$ rad/s, $\alpha_t = 4.14 \times 10^{-6}$ K^{-1}, $\rho = 2{,}330$ kg m^{-3}, $C^* = 695$ J kg^{-1} K^{-1}, $T_0 = 800$ K, $\tau_0 = 0.7$, $x = 0.5$, $\xi = -1$, $p_1 = 1 \times 10^{-2}$, $p_2 = 2 \times 10^{-2}$, $\tau = 5 \times 10^{-5}$, $d_n = -9 \times 10^{-31}$, $D_E = 2.5 \times 10^{-3}$, $E_g = 1.11$, $t = 0.5$.

Following Khalili [35], the double porous parameters are considered as $\alpha = 1.3 \times 10^{-5}$ N, $b_1 = 0.12 \times 10^{-5}$ N, $\gamma = 1.1 \times 10^{-5}$ N m^{-2}, $\gamma_1 = 0.16 \times 10^5$ N m^{-2}, $\gamma_2 = 0.219 \times 10^5$ N m^{-2}, $d = 0.1 \times 10^{10}$ N m^{-2}, $b = 0.9 \times 10^{10}$ N m^{-2}, $K_2 = 0.1546 \times 10^{-12}$ N m^{-2}, $K_1 = 0.1456 \times 10^{-12}$ N m^{-2}.

To solve the issue, we utilized the numerical technique described above to distribute the real part of the temperature T, the components of displacement u_1, u_3, the components of stress τ_{xx}, τ_{xz}, τ_{zz}, and the components of double porosity σ and τ. The outcome is a non-dimensional form of all the variables.

Figure 2 shows a comparison between the three different values of the thermoelastic coupling parameter ε_1. The first case when $\varepsilon_1 = 0.0017$, indicated by red color (—), the second case when $\varepsilon_1 = 0.0027$, indicated by green color (– – –), and the third case when $\varepsilon_1 = 0.0037$ (·····) on the physical fields under study. All results are for $\varepsilon_3 = -1.4 \times 10^{-36}$ and $H_0 = 10^5$ under the effect of a magnetic field with double porosity. In this figure (u_1, u_2, ϕ, ψ, τ_{xx}, τ_{xz}, τ_{zz}, τ_3, σ_3, and T), the variation in the thermoelastic coupling parameter results in different values being observed, but the carrier density N does not have an effect. The application of a logarithmic transformation is

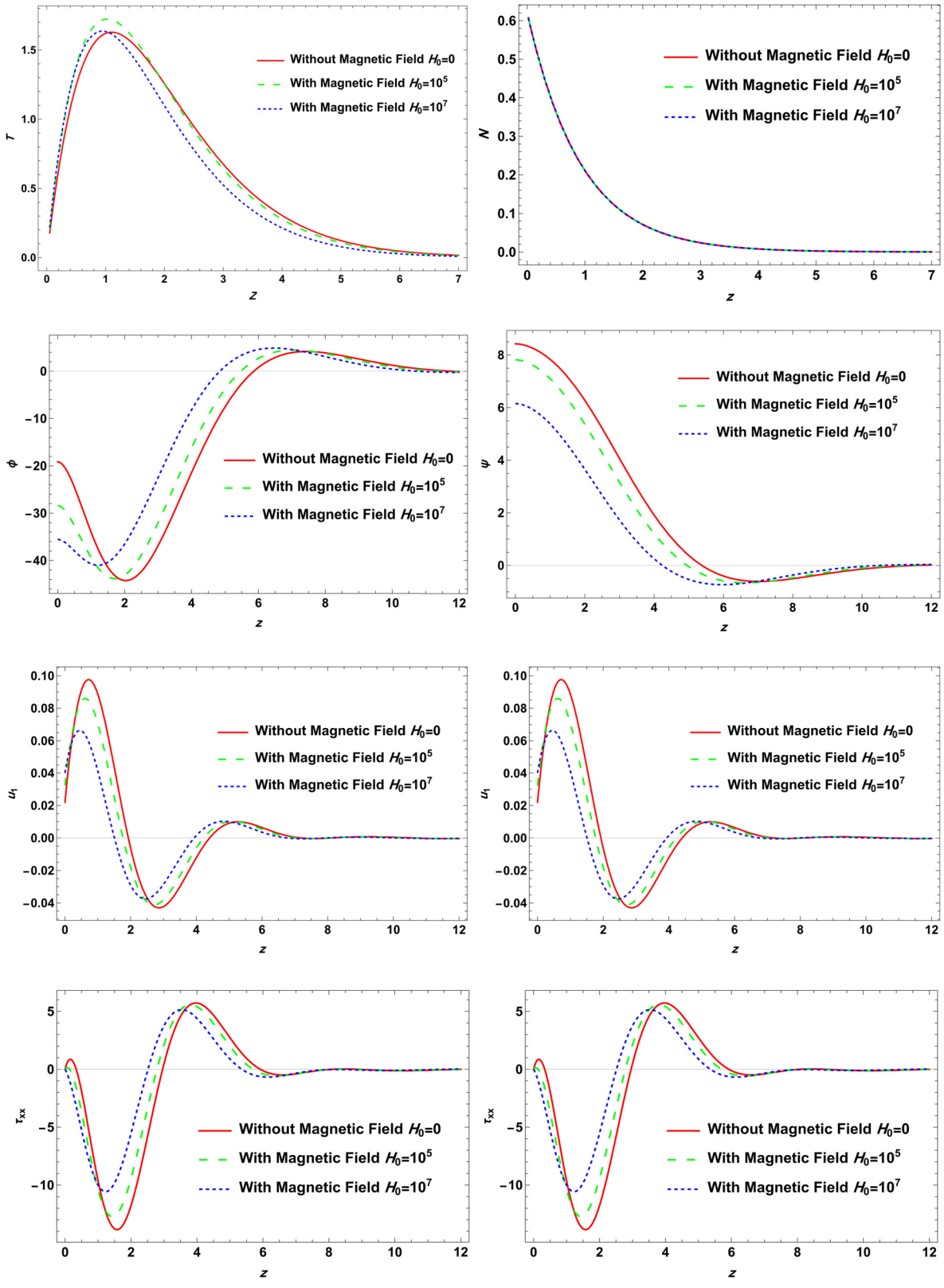

Figure 4: Variation in physical field distributions with distance at different magnetic field H_0 values when ε_1 = 0.0017 with double porosity.

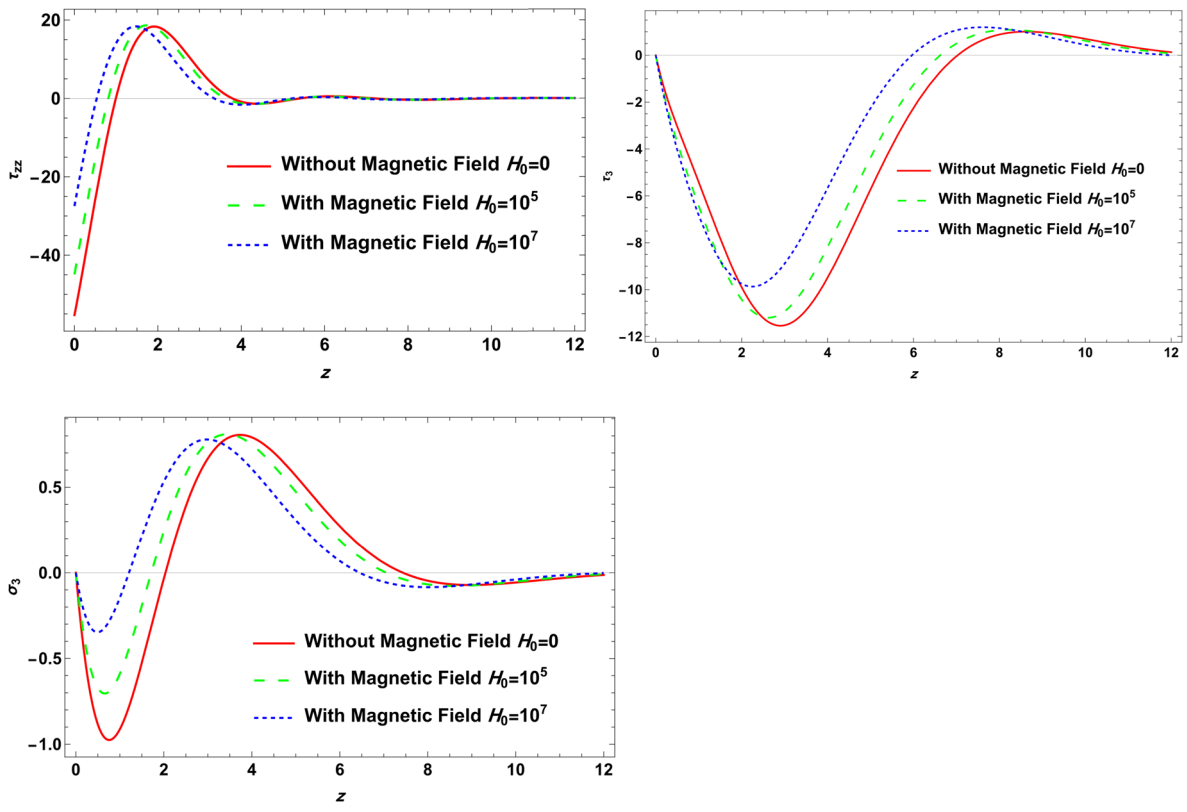

Figure 4: (*Continued*)

particularly useful for capturing variations in temperature and stress distributions over a wide range, aligning with similar methodologies presented in recent studies (*e.g.*, Seem and Singhal [27]). The logarithmic scale improves the clarity of trends in regions where small-scale behavior is critical, thereby enhancing the interpretability of the graphical results. Figure 3 illustrates the primary physical fields as a function of horizontal distance z within the framework of PT theory and L-S theory with double porosity. The results are evaluated in the presence of an external magnetic field when $\varepsilon_1 = 0.0017$ (Si). All curves discuss three cases of ε_3. The solid line (—) represents $\varepsilon_3 = -1.4 \times 10^{-36}$, the line (– – –) shows when $\varepsilon_3 = -2.4 \times 10^{-36}$, and the dotted lines (·····) show when $\varepsilon_3 = -3.4 \times 10^{-36}$. From the subfigure, it is clear that the variation in the thermoelectric coupling parameter has a great effect on all physical quantities, except that the carrier density has no impact, as it starts at a positive minimum and approaches the thermal insulation condition, and the temperature rises gradually. These plots align with the approach discussed in the study of Seema and Singhal [27]. Owing to the combination of an external magnetic field and photoexcitation, it quickly rises from the initial range to its surface maximum value. Conversely, for the other distributions, it is clear that the behavior of temperature, displacement, elastic waves, double porosity, stress force, and temperature distributions is greatly influenced by the thermoelectric coupling parameter. However, it does not have a discernible effect on carrier density distribution. Figure 4 illustrates the primary physical fields as a function of horizontal distance z within the framework of PT theory and L-S theory with double porosity. The results are evaluated in the presence of an external magnetic field for $\varepsilon_1 = 0.0017$ (Si). All curves discuss three cases for H_0. The solid line (—) represents $H_0 = 0$ (in the absence of a magnetic field), the line (– – –) shows when $H_0 = 10^5$, and the dotted lines (·····) show when $H_0 = 10^7$. From the subfigure, it is clear that the variation in the magnetic field has a great effect on all physical quantities, except that the carrier density has no impact. Figure 5 shows three-dimensional (3D) graphs between the time and distance with different physical quantities. Figure 6 introduces some samples of 3D heat maps. Temperature distribution shows variations in temperature using a red-yellow heat map, and stress distribution displays stress variations with a blue-red color scale.

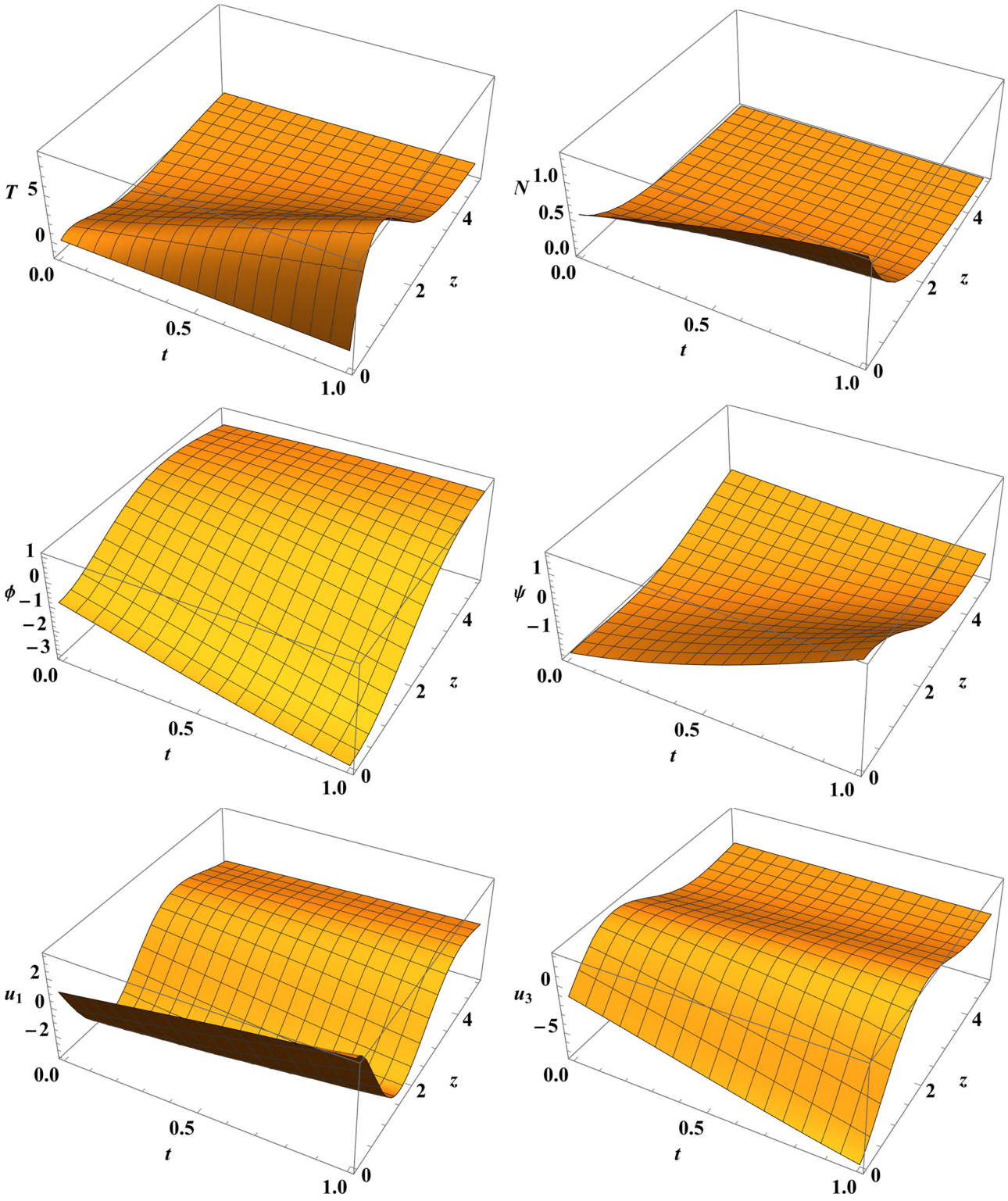

Figure 5: 3D graphs of physical field distributions with distance and time.

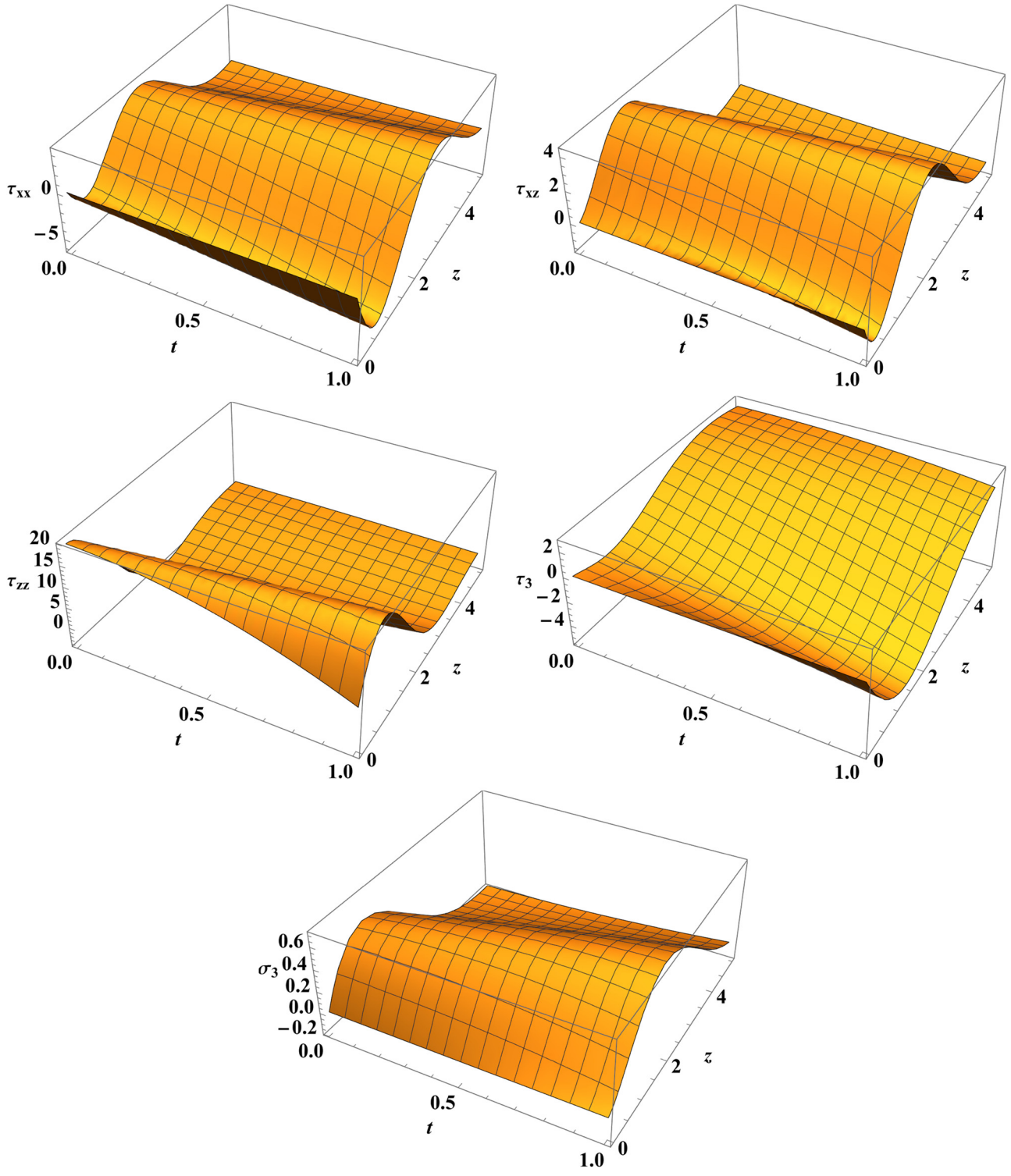

Figure 5: (*Continued*)

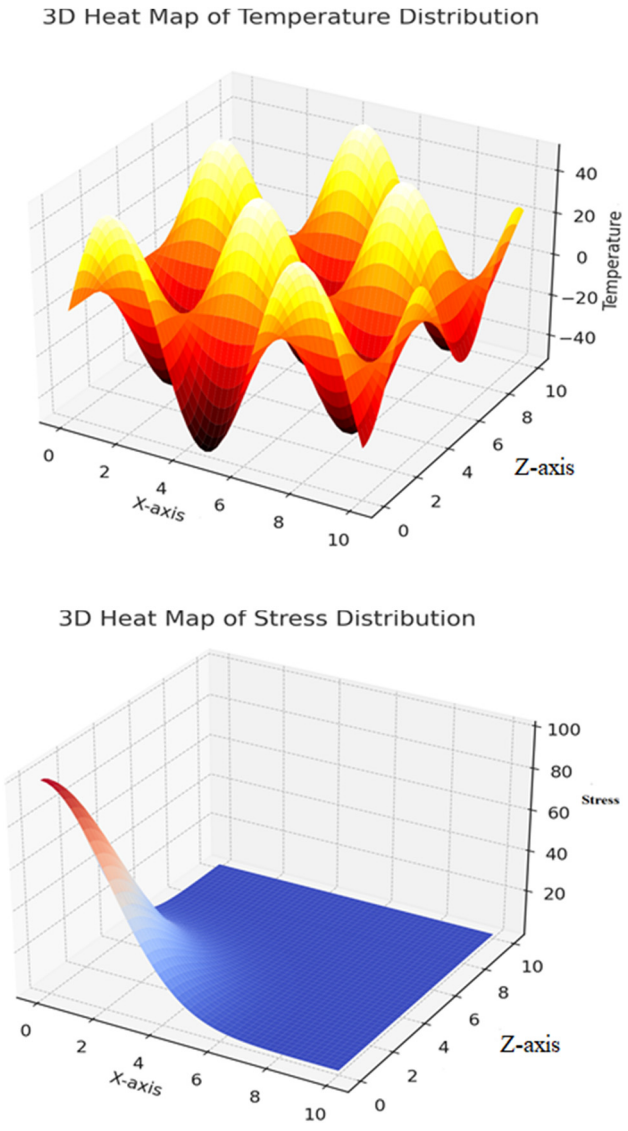

Figure 6: Heat map for temperature and stress distributions.

5.1 Validation

To ensure the accuracy and reliability of the proposed model, we validate our numerical results by comparing them with the existing theoretical and experimental data from the literature (Table 1). Specifically, we compare our results with those obtained in previous studies that analyze similar thermoelastic and double-porosity systems [42].

First, when the magnetic field parameter is set to zero, our results align closely with those reported by Abdou *et al.* [43], who studied generalized thermoelastic media with double porosity under the L-S's theory. This confirms the consistency of our model in the absence of an external magnetic field.

Furthermore, if both the magnetic field and the double-porosity effects are neglected, our findings reduce to the results obtained by Lotfy *et al.* [42] in the context of classical photo-thermoelasticity. The agreement between these cases demonstrates the robustness and adaptability of our model under different physical conditions.

The numerical comparisons indicate that the computed results, including displacement, stress, temperature, and porosity variations, exhibit a strong correlation with previously established findings. This validation confirms the effectiveness of our analytical approach and numerical implementation in capturing the complex interactions of thermoelasticity, magnetoelasticity, and double-porosity effects in semiconductor materials.

By successfully reproducing known results in limiting cases, our study provides confidence in the applicability of the proposed model for analyzing magneto-photo-thermoelastic interactions in double-porous media.

Table 1 highlights the consistency of our results with previous studies, reinforcing the validity of our model and its applicability to different physical scenarios.

6 Discussion and conclusion

The study has examined a novel mathematical model of the L-S theory within photo-thermoelastic theory, considering the effects of the magnetic field and double porosity. The research investigates the impact of thermoelastic and thermoelectric coupling parameters and magnetic fields on various physical phenomena within the problem. The external magnetic field affects the transmission of fundamental physical fields. The propagation of waves is regulated by the interplay of coupled photo-thermoelasticity, magnetic fields, dual porosity, and the physical constants of the material. The relationship between thermoelastic and thermoelectric properties is evident within the framework of photo-thermoelastic theory.

Table 1: Comparison of numerical results with previous studies

Study	Considered effects	Key findings	Agreement with present work
Abdou *et al.* [44]	Double porosity, no magnetic field	Thermoelastic behavior in double-porous media	Strong agreement
Lotfy *et al.* [42]	No magnetic field, no double porosity	Classical photo-thermoelastic response	Strong agreement
Present study	Magnetic field, double porosity	Magneto-photo-thermoelastic interactions	

To enhance the analysis, logarithmic scaling has been introduced in Figure 2 for the horizontal axis, allowing a more comprehensive visualization of parameter variations across different scales. The application of a logarithmic transformation is particularly useful for capturing variations in temperature and stress distributions over a wide range, aligning with similar methodologies presented in recent studies, such as Seem and Singhal [27]. The logarithmic scale improves the clarity of trends in regions where small-scale behavior is critical, thereby enhancing the interpretability of the graphical results.

6.1 Clarification of double porosity

In this study, double porosity refers to a material possessing two distinct pore systems, typically classified as macropores and microfissures. Macropores are larger cavities that dominate bulk fluid flow, while microfissures are smaller cracks or pores within the material. This dual-porosity structure leads to complex mechanical and thermal responses, affecting how waves propagate and stress is distributed within the material [44,45].

The presence of double porosity significantly influences the behavior of materials in engineering and geophysical applications. In porous geological formations, such as oil reservoirs and aquifers, the interaction between macropores and microfissures controls fluid transport, stress distribution, and wave propagation, making this concept crucial for enhancing oil recovery and geothermal energy extraction. Similarly, in biomedical engineering, porous materials with double porosity are used in bone implants and tissue scaffolds, where controlling the mechanical properties and fluid permeability is essential for biological integration. Furthermore, in semiconductor and nanotechnology applications, structured porous materials play a key role in thermal management and electronic cooling systems. By incorporating double porosity into our analysis, this study provides a deeper understanding of wave interactions in complex media, offering insights applicable to diverse scientific and industrial fields [46–48].

Furthermore, we analyze the physical significance of the studied parameters and their impact on the half-space behavior:

- *Thermoelastic and thermoelectric coupling*: The thermoelastic coupling parameter governs the interaction between thermal and mechanical fields. Higher values lead to increased thermal stresses and temperature gradients, causing stronger mechanical deformations. This behavior is particularly relevant in applications such as *geothermal energy extraction and high-temperature electronic materials*, where managing thermal expansion is crucial.
- *Magnetic field influence:* The applied magnetic field introduces *Lorentz forces*, which act as a damping mechanism on mechanical oscillations and wave propagation. This effect is critical in *semiconductor applications and electromagnetic shielding materials*, where reducing unwanted vibrations enhances stability and performance.
- *Double porosity and wave propagation*: The presence of two distinct pore systems significantly modifies wave speeds and stress distributions. This insight is essential for *oil reservoir modeling and carbon sequestration*, where understanding wave behavior in porous formations can optimize resource extraction techniques.
- *Geometrical considerations*: The depth and spatial extent of porosity variations influence stress concentrations and fracture propagation. This effect is particularly relevant in *earthquake modeling and rock mechanics*, where stress accumulation can lead to seismic activity and structural failures.

6.2 Real-world applications

The findings of this study have significant implications in various engineering and technological domains, including:

1) *Geophysics and earthquake engineering*: Understanding wave propagation in double-porous materials helps improve seismic wave analysis and earthquake prediction models, which are critical for designing safer infrastructure in earthquake-prone regions.
2) *Oil and gas industry:* The study provides insights into fluid dynamics in reservoir rocks, enhancing techniques for oil recovery and carbon sequestration by modeling how waves and stresses interact in porous geological formations.
3) *Semiconductor and nanotechnology:* The integration of magneto-photo-thermoelastic effects is valuable for optimizing semiconductor devices, including photonic and optoelectronic sensors used in precision applications.
4) *Biomedical engineering:* Double-porosity structures with thermoelastic properties can be utilized in biomedical implants, particularly for materials that require enhanced stress distribution and controlled thermal expansion.
5) *Aerospace and structural health monitoring*: Magnetic and thermal effects in porous materials play a crucial role in the design of lightweight, thermally stable materials for aerospace structures and real-time structural health monitoring systems.

Neglecting the effects of the external magnetic field and photothermal stimulation, the research findings underscore the importance of thermoelectric, thermoelastic, and magnetic fields in various modern geophysical engineering applications, such as solar cells, display technologies, and electrical circuits. Magnetic fields substantially influence the precision of measuring displacement, tension, and strain. Phase delays substantially affect all distributions [48,49].

The main aim of this work is to examine the effect of a magnetic field on a medium characterized by dual porosity levels, particularly with L-S's theory. The investigation aims to determine the extent to which the magnetic field influences the amplitude of certain physical parameters, either by enhancing or diminishing them. The data were acquired by contrasting the twofold porosity with and without a magnetic field. This comparison unveiled noteworthy instances. The normal mode method has been utilized to ascertain general solutions, which yield accurate responses by converting partial differential equations into ordinary differential equations through the implementation of boundary conditions. Programming enables us to observe the functionality of functions at certain values. The MATHEMATICA program was used to calculate numerical solutions. When exposed to a magnetic field, the differences between the existence and non-existence of double porosity are significant. All the physical quantities satisfy the boundary requirements. All physical quantities tend towards zero, and all functions exhibit continuity.

While this problem is theoretical, it can provide useful insights for experimental researchers in the domains of geophysics, earthquake engineering, and seismology, especially those who are studying mining tremors and drilling into the Earth's crust. Applying numerical approaches to solve the system of equations and conditions that govern the phenomenon can help overcome the limitations of the normal modes technique. This undertaking is currently in progress. The importance of this problem lies in its potential to improve our understanding of complex material behaviors, leading to innovations in the design and application of advanced materials in a variety of high-tech fields.

We examined the thermoelastic and fluid flow behavior of a double-porosity material under a magnetic field and the effects of many dominant factors. The parameters include thermoelastic, thermoelectric, and magnetic field intensity coupling parameters. First, thermal and elastic fields interact *via* the thermoelastic coupling parameter. Our results indicate that higher values increase thermal stresses and temperature-deformation field coupling. This increases displacement amplitudes and stress concentrations at the free surface. Geothermal energy extraction materials with higher porosity are more vulnerable to heat cracking, which improves the fracture fluid flow. Controlling helps biomedical device materials like thermal actuators and sensors respond reliably to thermal stimuli. Second, the thermoelectric coupling parameter controls the thermal–electric field interaction. We found that higher values increase thermal energy conversion into electric energy, carrier density (N), and heat transfer. Semiconducting materials, where thermoelectric coupling is crucial to energy harvesting, exhibit this phenomenon. Optimization improves thermal-to-electric energy conversion in solar cells. In electronic cooling systems, customized materials improve heat dissipation and prevent overheating. Finally, through the Lorentz force and induced electric fields, the magnetic field intensity greatly affects the material reaction. Our study shows that the opposing Lorentz force dampens elastic waves and reduces displacement amplitudes. Higher magnetic fields reduce stress concentrations at the free surface. Magnetic field sensors use controlled materials to detect and quantify magnetic fields precisely. Aerospace engineering uses magnetic fields to stabilize thermal and mechanical loads.

Acknowledgments: The authors would like to extend their sincere appreciation to Ongoing Research Funding program (ORF-2025-1112), King Saud University, Riyadh, Saudi Arabia.

Funding information: The project was funded under Project number (ORF-2025-1112).

Author contributions: All authors have accepted responsibility for the entire content of this manuscript and approved its submission.

Conflict of interest: The authors state no conflict of interest.

Data availability statement: The datasets generated and/or analyzed during the current study are available from the corresponding author on reasonable request.

References

[1] Biot MA. Mechanics of deformation and acoustic propagation in porous media. J Appl Phys. 1962;33(4):1482–98. doi: 10.1063/1.1728759.

[2] Detournay E, Cheng AHD. Fundamentals of poroelasticity. Compr Rock Eng: Princ Pract Proj. 1993;2:113–71.

[3] Pal SK, Maiti S. Thermoelastic response of a thin circular disk of double porosity under axisymmetric thermal shock. J Therm Stresses. 2001;24(6):509–28. doi: 10.1080/014957301300004494.

[4] Rice JR, Cleary MP. Some basic stress diffusion solutions for fluid-saturated elastic porous media with compressible constituents. Rev

Geophys Space Phys. 1976;14(2):227–41. doi: 10.1029/RG014i002p00227.
[5] Zhao J, Wang Y. Photothermoelastic analysis of a multilayered composite cylinder with functionally graded material and double porosity. Int J Mech Sci. 2020;184:105763. doi: 10.1016/j.ijmecsci.2020.105763.
[6] Lord H, Shulman Y. A generalized dynamical theory of thermoelasticity. J Mech Phys Solids. 1967;15:299–309.
[7] Barrenblatt G, Zheltov I, Kockina I. Basic concepts in the theory of seepage of homogeneous liquids in fissured rocks (Strata). Prikl Mat Mekh (Engl Translation). 1960;24:1286–303.
[8] Barrenblatt G, Zheltov I. On the basic equations of seepage of homogeneous liquids in fissured rock. Akad Nauk SSSR (Engl Translation). 1960;132:545–8.
[9] Khalili N, Valliappan S. Unified theory of flow and deformation in double porous media. Eur J Mech A, Solids. 1996;15:321–36.
[10] Masters I, Pao W, Lewis R. Coupling temperature to a double-porosity model of deformable porous media. Int J Numer Methods Eng. 2000;49:421–38.
[11] Khalili N, Selvadurai A. A fully coupled constitutive model for thermo-hydro-mechanical analysis in elastic media with double porosity. Geophys Res Lett. 2003;30(24):2268.
[12] Zhao Y, Chen M. Fully coupled dual-porosity model for anisotropic formations. Int J Rock Mech Min Sci. 2006;43(7):1128–33.
[13] Svanadze M. Dynamical problems of the theory of elasticity for solids with double porosity. Proc Appl Math Mech. 2010;10:309–10.
[14] Ainouz A. Homogenized double porosity models for poro-elastic media with interfacial flow barrier. Math Bohem. 2011;136:357–65.
[15] Svanadze M. Plane waves and boundary value problems in the theory of elasticity for solids with double porosity. Acta Appl Math. 2012;122:461–71.
[16] Straughan B. Stability and uniqueness in double porosity elasticity. Int J Eng Sci. 2013;65:1–8.
[17] Mahato CS, Biswas S. State space approach to characterize Rayleigh waves in nonlocal thermoelastic medium with double porosity under three-phase-lag model. Comput Math Math Phys. 2024;64(3):555–84.
[18] Berryman JG, Wang HF. The elastic coefficients of double-porosity models for fluid transport in jointed rock. J Geophys Res: Solid Earth. 1995;100(B12):24611–27. doi: 10.1029/95JB02665.
[19] Lewis RW, Schrefler BA. The finite element method in the deformation and consolidation of porous media. New York: John Wiley & Sons; 1998.
[20] Marin M, Marinescu C. Thermoelasticity of initially stressed bodies, asymptotic equipartition of energies. Int J Eng Sci. 1998;36(1):73–86.
[21] Florea OA. The backward-in-time problem of double porosity material with microtemperature. Symmetry. 2019;11(4):552.
[22] Kumar D, Singh D, Tomar SK. Surface waves in layered thermoelastic medium with double porosity structure: Rayleigh and Stoneley waves. Mech Adv Mater Struct. 2022;29(18):2680–705.
[23] Arusoaie A. Spatial and temporal behavior in the theory of thermoelasticity for solids with double porosity. J Therm Stresses. 2018;41(4):500–21.
[24] Rana N, Sharma DK, Sharma SR, Sarkar N. Effect of electromagnetic field on vibrations of nonlocal elastic cylinders with double porosity. J Vib Eng Technol. 2024;12(1):427–39. doi: 10.1007/s42417-024-01424-x
[25] Kumar R, Vohra R. Response of thermoelastic microbeam with double porosity structure due to pulsed laser heating. Mech Mech Eng. 2019;23(1).
[26] Seema S, Singhal A. Study of surface wave velocity in distinct rheological models with flexoelectric effect in piezoelectric aluminium nitride structure. J Braz Soc Mech Sci Eng. 2025;47:29. doi: 10.1007/s40430-024-05296-w.
[27] Seema S, Singhal A. Examining three distinct rheological models with flexoelectric effect to investigate Love-type wave velocity in bedded piezo-structure. Z Angew Math Mech. 2024;104:202400724. doi: 10.1002/zamm.202400724.
[28] Seema S, Singhal A. Mechanics of SH and anti-plane SH waves in orthotropic piezoelectric quasicrystal with multiple surface effect. Acta Mech. 2025;236:439–56. doi: 10.1007/s00707-024-04162-z.
[29] Seema S, Singhal A. Surface effects study: a continuum approach from fundamental modes to higher modes and topological polarization in orthotropic piezoelectric materials. J Appl Mech. 2025;92(1):011008. doi: 10.1115/1.4067204.
[30] Oreyeni T, Shamshuddin M, Obalalu A, Saeed A, Shah N. Exploring the impact of stratification on the dynamics of bioconvective thixotropic fluid conveying tiny particles and Cattaneo-Christov model: Thermal storage system application. Propuls Power Res. 2024;13(3):416–32. doi: 10.1016/j.jppr.2024.08.002.
[31] Shamshuddin M, Panda S, Pattnaik P, Mishra S. Ferromagnetic and Ohmic effects on nanofluid flow via permeability rotative disk: significant interparticle radial and nanoparticle radius. Phys Scr. 2024;99:055206. doi: 10.1088/1402-4896/ad35f8.
[32] Lotfy K, Elidy ES, Tantawi RS. Photothermal excitation process during hyperbolic two-temperature theory for magneto-thermo-elastic semiconducting medium. Silicon. 2021;13:2275–88.
[33] El-Sapa S, Lotfy K, Elidy ES, El-Bary A, Tantawi RS. Photothermal excitation process in semiconductor materials under the effect moisture diffusivity. Silicon. 2023;15(10):4171–82.
[34] El-Sapa S, Lotfy K, Elidy ES, Tantawi RS. Photothermal excitation process in semiconductor materials under the effect moisture diffusivity. Silicon. 2023;15:4171–82. doi: 10.1007/s12633-023-02311-y.
[35] Khalili N. Coupling effects in double porosity media with deformable matrix. Geo Res Lett. 2003;30(22):2153–5.
[36] Ieşan D, Quintanilla R. On a theory of thermoelastic materials with a double porosity structure. J Therm Stress. 2014;37:1017–36.
[37] Marin M, Lupu M. On harmonic vibrations in thermoelasticity of micropolar bodies. J Vib Control. 1998;4(5):507–18. doi: 10.1177/107754639800400501.
[38] Marin M, Abbas I, Kumar R. Relaxed Saint-Venant principle for thermoelastic micropolar diffusion. Struct Eng Mech. 2014;51(4):651–62.
[39] Marin M. Lagrange identity method for microstretch thermoelastic materials. J Math Anal Appl. 2010;363(1):275–86. doi: 10.1016/j.jmaa.2009.08.045.
[40] Bhatti MM, Marin M, Ellahi R, Fudulu IM. Insight into the dynamics of EMHD hybrid nanofluid (ZnO/CuO-SA) flow through a pipe for geothermal energy applications. J Therm Anal Calorim. 2023;148:14261–73. doi: 10.1007/s10973-023-12565-8.
[41] Yadav A, Carrera E, Marin M, Othman M. Reflection of hygrothermal waves in a Nonlocal Theory of coupled thermo-elasticity. Mech Adv Mater Struct. 2024;31(5):1083–96. doi: 10.1080/15376494.2024.
[42] Lotfy K, Mahdy AMS, El-Bary AA, Elidy ES. Magneto-photo-thermoelastic excitation rotating semiconductor medium based on moisture diffusivity. CMES-Comput Model Eng Sci. 2024;141(1):107–26.
[43] Abdou MA, Othman MI, Tantawi RS, Mansour NT. Exact solutions of generalized thermoelastic medium with double porosity under L–S theory. Indian J Phys. 2020;94:725–36.
[44] Abdou MA, Othman MI, Tantawi RS, Mansour NT. Effect of magnetic field on generalized thermoelastic medium with double porosity structure under L–S theory. Indian J Phys. 2020;94:1993–2004.

[45] Aljadani MH, Zenkour AM. Effect of magnetic field on a thermoviscoelastic body via a refined two-temperature Lord–Shulman model. Case Stud Therm Eng. 2023;49:103197. doi: 10.1016/j.csite.2023.103197.
[46] Heydarpour Y, Malekzadeh P, Gholipour F. Thermoelastic analysis of FG-GPLRC spherical shells under thermo-mechanical loadings based on Lord-Shulman theory. Compos Part B: Eng. 2019;164:400–24. doi: 10.1016/j.compositesb.2018.12.073.
[47] Kheibari F, Beni YT, Golestanian H. On the generalized flexothermoelasticity of a microlayer. Acta Mech. 2024;235:3363–84. doi: 10.1007/s00707-024-03884-4.
[48] Pakdaman M, Tadi Beni Y. Size-dependent Generalized Piezothermoelasticity of Microlayer. J Appl Comput Mech. 2025;11(1):223–38. doi: 10.22055/jacm.2024.46393.4510.
[49] Kheibari F, Beni YT, Kiani Y. Lord-Shulman based generalized thermoelasticity of piezoelectric layer using finite element method. Struct Eng Mech. 2024;92(1):81–8. doi: 10.12989/sem.2024.92.1.081.